Title: Rab11 suppresses neuronal stress signaling by localizing Dual leucine zipper kinase to axon terminals for protein turnover.

Seungmi Kim, Yaw Quagraine, Monika Singh, Jung Hwan Kim*

Department of Biology, University of Nevada, Reno, Reno, NV 89557

*Correspondence: jungkim@unr.edu

Summary

Dual Leucine Zipper Kinase (DLK) mediates multiple neuronal stress responses, and its expression levels are constantly suppressed to prevent excessive stress signaling. We found that Wallenda (Wnd), the *Drosophila* ortholog of DLK, is highly enriched in the axon terminals of *Drosophila* sensory neurons in vivo and that this subcellular localization is necessary for Highwire-mediated Wnd protein turnover under normal conditions. Our structure-function analysis found that Wnd palmitoylation is essential for its axon terminal localization. Palmitoylation-defective Wnd accumulated in neuronal cell bodies, exhibited dramatically increased protein expression levels, and triggered excessive neuronal stress responses. Defective intracellular transport is implicated in neurodegenerative conditions. Comprehensive dominant-negative Rab protein screening identified Rab11 as an essential factor for Wnd localization in axon terminals. Consequently, *Rab11* loss-of-function increased the protein levels of Wnd and induced neuronal stress responses. Inhibiting Wnd activity significantly ameliorated neuronal loss and c-Jun N-terminal kinase signaling triggered by *Rab11* loss-of-function. Taken together, these suggest that DLK proteins are constantly transported to axon terminals for protein turnover and a failure of such transport can lead to neuronal loss. Our study

demonstrates how subcellular protein localization is coupled to protein turnover for neuronal stress signaling.

Keywords

DLK, Wallenda, Rab11, axon terminals, protein turnover, Highwire, protein palmitoylation, neurodegeneration

Highlights

- Wnd is highly enriched in axon terminals.
- Wnd protein turnover by Hiw is restricted in the axon terminals.
- Protein palmitoylation of Wnd and Rab11 activity is essential for Wnd axonal localization.
- *Rab11* mutations and defective Wnd palmitoylation impair Wnd protein turnover leading to increased Wnd protein levels and neuronal loss.
- Inhibiting Wnd activity mitigates neuronal stress response caused by *Rab11* loss-of-function.

39 Introduction

40 A typical neuron is composed of distinct somatodendritic and axonal compartments that express
41 unique compositions of membrane and cytoplasmic proteins, which are precisely established
42 and maintained through a complex network of intracellular transport processes (Guedes-Dias
43 and Holzbaur, 2019; Guillaud et al., 2020). Consistently, impaired neuronal intracellular
44 transport has been recognized as an early cellular event in various neurodegenerative disorders
45 including amyotrophic lateral sclerosis (Collard et al., 1995; De Vos and Hafezparast, 2017),
46 Alzheimer's (Calkins et al., 2011; Wang et al., 2015), Parkinson's (Saha et al., 2004; Chu et al.,
47 2012), and Huntington's diseases (Lee et al., 2004; Reddy and Shirendeb, 2012; Smith et al.,
48 2014). The intricate regulation of intracellular transport relies on a family of small G proteins
49 known as Rab (Ras-related in brain) proteins (Stenmark, 2009). Studies have demonstrated
50 altered Rab activity or expression levels in Huntington's disease model (Li et al., 2009b, 2009a),
51 Alzheimer's disease model (Pensalfini et al., 2020) and from the amyotrophic lateral sclerosis
52 patients (Mitra et al., 2019). However, how defective neuronal intracellular transport leads to
53 neuronal loss is not fully understood.

54 Dual Leucine Zipper Kinase (DLK), also known as MAP3K12 is a cytoplasmic protein kinase
55 essential for stress signaling and mediates diverse neuronal responses including axon
56 regeneration, axon degeneration, and cell death (Miller et al., 2009; Xiong et al., 2010; Shin et
57 al., 2012; Xiong and Collins, 2012; Watkins et al., 2013; Li et al., 2021). Under normal
58 conditions, neurons tightly control DLK activity to prevent excessive stress signaling primarily
59 through protein turnover by an evolutionarily conserved PHR1/RPM-1/Highwire (Hiw) ubiquitin
60 ligases (Nakata et al., 2005; Collins et al., 2006; Xiong et al., 2010; Huntwork-Rodriguez et al.,
61 2013). Notably, recent studies have shown potential widespread involvement of DLK in neuronal
62 death observed in neurotrophic factor deprivation, glaucoma, amyotrophic lateral sclerosis, and
63 Alzheimer's disease models (Pozniak et al., 2013; Welsbie et al., 2013, 2017; Larhammar et al.,

2017a; Le Pichon et al., 2017; Patel et al., 2017). These observations suggest the possibility of dysregulated or elevated DLK protein/activity levels in these conditions. Interestingly, DLK proteins are found within axonal compartments (Xiong et al., 2010; Klinedinst et al., 2013; Holland et al., 2016; Niu et al., 2020, 2022). However, there is limited understanding of the mechanisms underlying DLK protein localization in axonal compartments and how such axonal localization of DLK plays a role in neuronal stress responses.

Here, we report a novel coupling between axon terminal localization and protein turnover of DLK. We further found that Rab11 is essential for this coupling, which when disrupted, leads to neuronal loss by excessive stress signaling. We found that Wallenda (Wnd), *Drosophila* DLK is highly enriched in the axon terminals of *Drosophila* sensory neurons in vivo. Furthermore, we found that Wnd protein turnover by Hiw is confined to axon terminals. We identified a protein palmitoylation on Wnd as an essential motif for Wnd protein localization in axon terminals. By taking advantage of this unique behavior of *Drosophila* DLK, Wnd in its reliance to protein palmitoylation for axonal localization, we demonstrated that Wnd protein turnover is greatly diminished when Wnd proteins are not transported to axon terminals, which in turn causes excessive Wnd signaling and neuronal cell death. We further uncovered the selective role of Rab11 in Wnd axonal localization and protein turnover. Importantly, neuronal stress responses caused by *Rab11* loss-of-function were significantly mitigated by inhibiting Wnd. Together, our findings suggest that Rab11 suppresses DLK protein levels by coupling axonal localization and protein turnover of DLK.

85 Result

86 **Wnd is highly enriched in axon terminals and Wnd protein turnover is restricted to axon**
87 **terminals.**

88 DLK proteins are found in the axonal compartments of diverse animals (Holland et al., 2016; Niu
89 et al., 2020, 2022). To understand the mechanism of DLK axonal localization, we first set out to
90 investigate the extent of axonal localization of *Drosophila* DLK, Wallenda (Wnd). We took
91 advantage of a *wnd* protein-trap allele, *Mi{MIC}wnd*^{GFSTF}, which allows us to visualize
92 endogenous Wnd protein localization via an EGFP tag (Venken et al., 2011; Li et al., 2017).
93 The levels of Wnd-GFSTF proteins in the third instar larva stage were extremely low (**Figure**
94 **1A**, left). To enhance detection of Wnd-GFSTF, the experiment was performed in *highwire* (*hiw*)
95 mutants, *hiw*$^{\Delta N}$ (Wu et al., 2005). Hiw is a neuronal ubiquitin ligase that selectively targets Wnd
96 for protein degradation (Collins et al., 2006). Immunostaining was conducted using an anti-GFP
97 antibody, and the larval samples were examined using a confocal microscope. The result
98 showed a strikingly polarized expression pattern of Wnd. While Wnd-GFSTF expression was
99 evident in the neuropil region in the ventral nerve cord (VNC) (**Figure 1A and 1B**), we could not
100 detect any meaningful signal from neuronal cell bodies, especially from the peripheral nervous
101 system neurons. Neuropils are enriched in neuronal dendrites and axons, while neuronal cell
102 bodies are mostly absent in this region. This suggests that Wnd protein expression levels are
103 kept extremely low in neuronal cell bodies but enriched in neuronal processes likely in axon
104 terminals.

105 Next, we employed a transgene approach. We generated Wnd-GFP transgenes with and
106 without *wnd* mRNA's untranslated region (UTR), namely 5'UTR-Wnd::GFP-3'UTR and
107 Wnd::GFP to test a role of *wnd*-UTRs in Wnd protein localization. These transgenes were
108 expressed specifically in larval class IV dendritic arborization (C4da) neurons using the *ppk*-
109 GAL4 driver (Grueber et al., 2007). C4da neurons have their cell bodies positioned in the larval

110 body wall, where they extend dendrites and send axons to the VNC of the larval central nervous
111 system. This sensory neuron system provides an excellent opportunity for studying protein
112 localization in cell bodies, dendrites, and axon terminals (**Figure 1B**) (Grueber et al., 2007). We
113 quantified the expression levels of Wnd transgenes in the cell bodies and axon terminals of
114 C4da neurons using quantitative confocal microscope imaging. The expression levels were
115 normalized using a general membrane marker, mCD8::RFP. The expression levels of
116 mCD8::RFP in axon terminals may represent passive diffusion of membrane proteins, which
117 reports the absence of axonal enrichment or equals to the axonal enrichment of 1. We observed
118 a significant enrichment of Wnd in the axon terminals of C4da neurons, regardless of *wnd*-UTRs
119 (**Figure 1C** and **1D**). Overactive Wnd signaling impairs *ppk*-GAL4 activity, compounding our
120 analysis (Wang et al., 2013). To address this, we treated larvae with DLKi/GNE-3511, a specific
121 inhibitor of DLK/Wnd kinase activity (Patel et al., 2017; Russo and DiAntonio, 2019). The
122 treatment with DLKi did not affect larval viability or basal Cd4a morphology. Additionally, a
123 kinase-dead version of Wnd, Wnd-KD::GFP, exhibited similar axonal enrichment in comparison
124 to Wnd::GFP in the presence and absence of DLKi (**Figure 1 - supplement**).

125 What might be the biological significance of such high axon terminal enrichment of Wnd
126 proteins? Interestingly, a previous work has shown that nerve injury in *Drosophila* larvae
127 increased Wnd protein levels in proximal axons but not in motor neuron cell bodies (Xiong et al.,
128 2010), which suggests that injury signal does not affect Wnd protein levels in neuronal cell
129 bodies. Thus, we wondered whether Wnd protein degradation under normal conditions is also
130 compartment specific. To test this possibility, we expressed Wnd-KD::GFP in C4da neurons of
131 wild-type and *hiw* mutant animals ($hiw^{\Delta N}$). The expression levels of Wnd-KD::GFP was
132 measured in C4da cell bodies and C4da axon terminals by quantitative confocal microscope
133 imaging (**Figure 1E**). The result showed that *hiw* mutations did not change Wnd-KD::GFP
134 expression in C4da cell bodies as compared to a wild-type control. In contrast, there was a

135 remarkable 7-fold increase in Wnd-KD::GFP expression levels specifically in the axon terminals
136 in the presence of *hiw* mutations.

137 Taken together, these suggest that Wnd proteins are highly enriched in axon terminals and that
138 this axon terminal localization is a necessary step for Hiw-mediated Wnd protein turnover. DLK
139 proteins act as a sensor in neuronal stress responses, and under normal conditions, their
140 protein levels are constantly suppressed to prevent undesired stress responses (Nakata et al.,
141 2005; Collins et al., 2006; Xiong et al., 2010; Huntwork-Rodriguez et al., 2013). In this context, if
142 Wnd localization in axon terminals is disrupted, it may lead to dysregulated Wnd protein
143 expression levels, potentially resulting in exacerbated stress signaling. To test the model, we
144 decided to identify the mechanisms underlying Wnd localization in axon terminals.

145

146 **The protein palmitoylation of Wnd is essential for axonal localization of Wnd.**

147 The coding region of *wnd* was sufficient for Wnd axon terminal localization (**Figure 1**). Wnd
148 proteins are found on axonally transporting vesicles (Xiong et al., 2010). Together these further
149 suggest that Wnd protein localization in axon terminals are through axonal anterograde
150 transport of Wnd proteins, and that Wnd protein degradation is dependent on this axonal
151 anterograde transport. Protein transport often involves small protein domains or motifs. To find
152 the motifs necessary for axonal transport of Wnd, we performed a structure-function analysis by
153 progressively deleting 100 amino acids (aa) from Wnd transgenes (**Figure 2A**). These Wnd
154 transgenes were expressed in C4da neurons, and the axonal enrichment of Wnd was measured
155 as described in Figure 1D. Deletion of the first 100 aa of Wnd (WndΔ100::GFP) did not have an
156 impact on enrichment of Wnd in axon terminals. However, deleting the first 200 aa of Wnd
157 (WndΔ200::GFP) resulted in a dramatic 43-fold reduction of Wnd enrichment. Similarly, deleting
158 aa 101-200 of Wnd (WndΔ101-200::GFP) led to a dramatic decrease in Wnd localization in

159 axon terminals (**Figure 2B**). These findings suggest that the 101-200 aa region of Wnd contains
160 a crucial motif for axonal anterograde transport of Wnd.

161 Interestingly, this region contains an evolutionarily conserved palmitoylation motif, Cysteine-130
162 (Wnd-C130) (**Figure 2C**). Previous studies have shown that palmitoylation is required for DLK
163 association with neuronal vesicles and DLK signaling in cultured mammalian neurons and *C.*
164 *elegans* (Holland et al., 2016). However, whether DLK palmitoylation changes DLK protein
165 localization in axon terminals remains unknown. Additionally, whether Wnd undergoes protein
166 palmitoylation is not known. To examine the protein palmitoylation of Wnd, we introduced a
167 mutation changing the Cysteine to Serine, resulting in Wnd-C130S. We expressed wild-type
168 Wnd (Wnd::GFP) and the palmitoylation site mutant Wnd (Wnd-C130S::GFP) in cultured
169 *Drosophila* Schneider 2 (S2) cells using PEI-mediated transfection (Longo et al., 2013). The
170 Acyl-Biotin Exchange (ABE) assay (Drisdel et al., 2006) was conducted to measure protein
171 palmitoylation of Wnd proteins after pulldown using a GFP-tag. The results showed a 50%
172 reduction in protein palmitoylation in Wnd-C130S::GFP compared to Wnd::GFP (**Figure 2D**),
173 providing strong evidence that Wnd-C130 is a palmitoylation site. Subsequently, we expressed
174 Wnd::GFP and Wnd-C130S::GFP in larval C4da neurons and measured their axonal
175 enrichment. The findings revealed a dramatic 30-fold reduction in Wnd axonal localization for
176 Wnd-C130S::GFP compared to Wnd::GFP (**Figure 2E**). Taken together, our data demonstrates
177 that Wnd-C130 is palmitoylated in *Drosophila,* which is essential for Wnd localization in axon
178 terminals.

179 Interestingly, we noticed that unlike diffuse cytoplasmic expression patterns of palmitoylation-
180 defective DLK observed in mammalian cells (Holland et al., 2016), Wnd-C130S::GFP exhibited
181 discrete localization patterns in C4da cell bodies (**Figure 2E**). These structures extensively
182 colocalized with somatic Golgi complex (**Figure 2 – supplement 1**). In mammalian cultured
183 cells, DLK was found in somatic Golgi complex where its palmitoyltransferase, HIP14 localizes

184 (Niu et al., 2020). Consistently, we found that Wnd is localized to somatic Golgi complex in
185 C4da cell bodies, which required the 101-200 aa region of Wnd (**Figure 2 – supplement 2**).
186 *Drosophila* HIP14, dHIP14 showed somatic Golgi localization and extensive colocalization with
187 Wnd proteins in C4da cell bodies (**Figure 2 – supplement 3**). Furthermore, mutating *dHIP14*
188 significantly decreased Wnd enrichment in axon terminals (**Figure 2 – supplement 3**). These
189 suggest that Wnd protein palmitoylation is catalyzed by dHIP14 in somatic Golgi complex like
190 mammalian cells. However, unlike mammalian and *C. elegans* DLK proteins, Wnd
191 palmitoylation is not necessary for Golgi localization since Wnd-C130S::GFP retained Golgi
192 localization (**Figure 2 – supplement 1**). Moreover, Wnd palmitoylation plays a unique role in
193 localizing Wnd proteins in axon terminals in *Drosophila*.

194

195 **Palmitoylation-defective Wnd evades protein turnover and accumulates in neuronal cell**
196 **bodies.**

197 Wnd-C130S does not localize in the axon terminals but rather retained in neuronal cell bodies.
198 This may prevent protein turnover of Wnd-C130S, which may result in increased protein
199 expression levels of Wnd-C130S. To test the idea, we expressed Wnd::GFP and Wnd-
200 C130S::GFP using a pan-neuronal driver, *Elav*-GAL4. The larvae were treated with DLKi/GNE-
201 3511 to prevent lethality caused by overactive Wnd signaling. The total protein expression levels
202 of Wnd::GFP and Wnd-C130S::GFP were measured in larval brain lysates using Western blot
203 analysis with GFP antibody (**Figure 3A**). The results revealed a dramatic 7.1-fold increase in
204 protein levels of Wnd-C130S::GFP compared with Wnd::GFP. To determine the cellular
205 localization of increased Wnd-C130S::GFP expression, we expressed Wnd::GFP and Wnd-
206 C130S::GFP along with mCD8::RFP in larval C4da neurons using *ppk*-GAL4 and directly
207 compared the protein expression levels of the Wnd transgenes in C4da axon terminals and cell
208 bodies as measured by GFP fluorescent intensity (**Figure 3B**). We observed a dramatic 10-fold

209 increase in protein expression levels of Wnd-C130S::GFP in C4da cell bodies compared with
210 Wnd::GFP. On the other hand, Wnd-C130S::GFP exhibited greatly reduced protein expression
211 levels in C4da axon terminals (3-fold reduction) compared with Wnd::GFP. Together, these
212 findings strongly support the notion that Wnd localization in axon terminals is crucial for protein
213 turnover of Wnd.

214

215 **Palmitoylation-defective Wnd triggers excessive stress signaling and neuronal loss.**

216 DLK triggers neuronal stress signaling (Nakata et al., 2005; Collins et al., 2006; Karney-Grobe
217 et al., 2018). A failure to suppress Wnd protein levels in Wnd-C130S::GFP may lead to
218 excessive neuronal stress signaling. While the essential role of palmitoylation in DLK signaling
219 has been demonstrated in *C. elegans* and cultured mammalian cells (Holland et al., 2016;
220 Martin et al., 2019; Niu et al., 2020, 2022), its impact on the signaling capacity of Wnd remains
221 unknown. In contrast to the diffuse cytoplasmic expression pattern of palmitoylation-deficient
222 DLK proteins in worms and mammalian cells, Wnd-C130S::GFP exhibited clear somatic Golgi
223 localization (**Figure 2 – supplement 1**). A recent study suggested that the membrane
224 localization of DLK proteins, rather than palmitoylation itself, is crucial for DLK signaling (Tortosa
225 et al., 2022). Therefore, we investigated whether Wnd-C130S::GFP retains signaling capacity.
226 We expressed Wnd::GFP and Wnd-C130S::GFP in larval C4da neurons using *ppk-GAL4*. We
227 used *puc-lacZ,* a transcription reporter downstream of c-Jun N-terminal Kinase (JNK) as a proxy
228 for Wnd signaling (Martin-Blanco et al., 1998). Expression levels of *puc-lacZ* were evaluated by
229 immunostaining and its fluorescent intensity was measured in C4da nucleus. The results
230 showed robust induction of *puc-lacZ* by Wnd::GFP as well as by Wnd-C130S::GFP (**Figure 4 –**
231 **supplement 1A**). Additionally, the excessive axon arborization induced by Wnd signaling was
232 also observed both in Wnd::GFP and Wnd-C130S::GFP expressing C4da neurons. These were
233 dependent on Wnd kinase activity since there was no exuberant axon arborization by Wnd-

234 KD::GFP nor by Wnd-C130S-KD::GFP – the kinase dead versions of Wnd and Wnd-C130S
235 respectively (**Figure 4 – supplement 1B**). These strongly suggest that unlike DLK proteins in *C.*
236 *elegans* and mammalian cells, the palmitoylation of Wnd is not essential for signaling in
237 *Drosophila*.

238 Wnd-C130S::GFP exhibited 7-fold increase in protein expression levels compared to Wnd::GFP
239 (**Figure 3A**) while showing similar signaling capacity both in axon arborization and *puc-lacZ*
240 expression. We wondered if excessive transgene expression levels caused signaling pathway
241 saturation. Thus, we decided to reduce transgene expression levels. We recently have
242 generated a plasmid system for reduced transgene expression (Singh and Kim, 2022). Using
243 these plasmids, additional Wnd transgenes containing two UAS sites (2XUAS) rather than five
244 UAS sites (5XUAS) were generated and were expressed in larval C4da neurons. Then, *puc-*
245 *lacZ* expression levels were measured. The result showed that Wnd-C130S::GFP induced a
246 3.7-fold more *puc-lacZ* expression than Wnd::GFP when expressed under 2XUAS (**Figure 4A**).
247 This strongly suggests that Wnd-C130S::GFP triggers stronger stress signaling because it
248 cannot be transported towards axon terminals thus, evades protein turnover.

249 To determine whether this excessive Wnd signaling from Wnd-C130S::GFP results in neuronal
250 loss, we expressed Wnd-C130S::GFP and Wnd::GFP under *GMR-GAL4*, eye specific driver
251 (Seong et al., 2001). Expressing Wnd transgenes with 5XUAS caused complete lethality under
252 a standard growth condition for both Wnd::GFP and Wnd-C130S::GFP. Growing flies at a lower
253 temperature partially rescued lethality - likely due to lower transgene expression levels. Severe
254 eye loss phenotypes were observed from Wnd-C130S::GFP and Wnd::GFP expressing flies in
255 this experimental condition. We observed, albeit to a small extent, more severe eye loss
256 phenotypes in Wnd-C130S::GFP flies as compared to Wnd::GFP flies (**Figure 4 – supplement**
257 **2A and 2B**). To substantiate our findings, we expressed Wnd-C130S::GFP and Wnd::GFP
258 under 2XUAS using *GMR-GAL4*. Even with 2XUAS transgenes, animals expressing Wnd-

259 C130S::GFP showed significant lethality as compared to Wnd::GFP expressing animals (**Figure**
260 **4B**). Moreover, 100% of surviving flies of Wnd-C130S::GFP exhibited rough eye and eye
261 pigmentation loss phenotypes, which indicates loss of photoreceptors. On the other hand, flies
262 expressing 2XUAS-Wnd::GFP did not show any discernable phenotypes as compared to the
263 controls (**Figure 4C**). Wnd transgenes alone did not exhibit any defects in eye development.

264 These strongly suggest that axonal anterograde transport of Wnd is essential for Wnd protein
265 turnover and that a failure of this transport triggers excessive stress signaling.

266

267 **Selective involvement of Rab proteins in Wnd axonal localization.**

268 Protein palmitoylation enhances the hydrophobicity of target proteins, leading to increased
269 membrane association. This suggests that Wnd proteins are transported to axons through an
270 intracellular vesicular transport system. The regulation of intracellular vesicular transport is
271 governed by Rab proteins (Stenmark, 2009). To gain insights on axonal anterograde transport of
272 DLK proteins, we conducted a screening of Rab proteins to identify those that contribute to Wnd
273 axonal localization. We tested a total of 26 Rab proteins out of the 33 annotated *Drosophila* Rab
274 proteins (Zhang et al., 2007). YFP-tagged dominant-negative (DN) Rab proteins were
275 expressed along with RFP-fused Wnd-KD (Wnd-KD::mRFP) in C4da neurons. The axonal
276 enrichment of Wnd-KD::mRFP was analyzed by measuring the fluorescence intensities of Wnd-
277 KD::mRFP in C4da cell bodies and axon terminals (**Figure 5**). Among the tested DN-Rab
278 proteins, only Rab1 and Rab11 showed a significant reduction in Wnd axonal enrichment. These
279 findings suggest that Wnd targeting to axon terminals is a highly specific process. Rab1 is
280 involved in ER to Golgi traffic. The dramatic decrease in Wnd axonal localization observed upon
281 Rab1 inhibition is interesting as Wnd palmitoylation likely occurs at the somatic Golgi complex.
282 Rab11 regulates membrane traffic at the recycling endosome (Stenmark, 2009).

283

284 **Rab11 inhibition caused dysregulated Wnd protein levels.**

285 Rab11-positive recycling endosomes (REs) play a role in mediating anterograde Golgi-to-
286 plasma membrane trafficking (Ang et al., 2004; Satoh et al., 2005; Taguchi, 2013). This raises
287 an interesting possibility that once palmitoylated at the Golgi, Wnd is sorted at the REs for
288 axonal transport. To investigate this, we examined whether Wnd proteins are present at the REs
289 in C4da cell bodies. Wnd-KD::mRFP was expressed in C4da neurons, and the Rab11-positive
290 REs were labeled using endogenously tagged YFP::Rab11 (TI-YFP::Rab11) (Dunst et al.,
291 2015). We analyzed the portion of Wnd-KD::mRFP that colocalizes with YFP::Rab11 using the
292 Manders' Overlap Coefficient. The results showed extensive colocalization between Wnd-
293 KD::mRFP and YFP::Rab11 in C4da cell bodies (Manders' coefficient 0.60 ± 0.14) (**Figure 6A**).
294 Similar results were obtained with transgenic expression of YFP::Rab11 and Wnd-KD::mRFP
295 (Manders' coefficient 0.81 ± 0.11) (**Figure 6B**). On the other hand, we did not detect any
296 meaningful colocalization between YFP::Rab11 and Wnd-KD::mRFP in C4da axon terminals or
297 in axons (Manders' coefficient 0.34 ± 0.14 and 0.41 ± 0.10 respectively) (**Figure 6 –**
298 **supplement 1**). Scale bar = 3 μm. These suggest that Rab11 is involved in Wnd protein sorting
299 at the somatic REs rather than transporting Wnd directly.

300 If Rab11 is necessary for Wnd anterograde transport, inhibiting Rab11 may lead to dysregulated
301 Wnd protein turnover and increased Wnd protein levels. To test the idea, we expressed DN-
302 YFP::Rab11 along with Wnd-KD::mRFP in C4da neurons. We directly compared the expression
303 levels of Wnd-KD::mRFP in C4da cell bodies and axon terminals. A mCD8::GFP transgene was
304 used as a control for DN-Rab11. The results revealed a dramatic 4.2-fold increase in Wnd-
305 KD::mRFP expression levels in C4da cell bodies by DN-Rab11, but not in the axon terminals
306 (**Figure 6C**), which is reminiscent of Wnd-C130S behavior (**Figure 3B**).

307 We further examined the role of Rab11 in Wnd axonal localization using *Rab11* mutants,
308 *Rab11*^{93Bi}, which is a strong loss-of-function allele (Giansanti et al., 2007). Wnd-KD::GFP was

309 expressed along with mCD8::RFP in wild-type and homozygous *Rab11*^{93Bi} C4da neurons, and
310 the axonal enrichment of Wnd-KD::GFP was measured. The results showed a dramatic
311 reduction in Wnd axonal enrichment by *Rab11* mutations (**Figure 6D**). Next, we measured the
312 total expression levels of endogenous Wnd using Western blot analysis on brain lysates from
313 wild-type control and homozygous *Rab11*^{93Bi} larvae (**Figure 6E**). The results showed a
314 significant 2.8-fold increase in total Wnd protein levels by *Rab11* mutations. This increase in
315 Wnd protein levels was not due to increased *wnd* gene expression because *wnd* mRNA levels
316 were not increased by *Rab11* mutations (**Figure 6 - supplement 2**). Rather, it showed a
317 significant reduction in *wnd* mRNA, which may be caused by a possible negative feedback from
318 excessive Wnd signaling. Together, these findings strongly suggest that Rab11 mediates Wnd
319 protein transport out of neuronal cell bodies towards axon terminals and that a failure in this
320 transport leads to dysregulated Wnd protein turnover.

321

322 **Neuronal loss caused by Rab11 loss of function requires Wnd activity.**

323 A previous work has shown that *Rab11* mutations caused photoreceptor loss in *Drosophila* eye
324 and JNK signaling activation (Tiwari and Roy, 2009). However, how *Rab11* mutations induce
325 JNK signaling is not clear. One of the pathways leading to JNK activation is DLK/Wnd (Collins et
326 al., 2006; Xiong et al., 2010; Ghosh et al., 2011). Thus, we hypothesized that increased Wnd
327 expression contributes to the neuronal loss and JNK activation by *Rab11* loss-of-function. To
328 test the idea, we expressed DN-Rab11 along with a membrane marker mCD8::RFP in the larval
329 C4da sensory neurons using *ppk-GAL4* (Grueber et al., 2007). JNK activation was monitored by
330 *puc-lacZ* induction (Martin-Blanco et al., 1998). The result showed a 2.8-fold increase of *puc-*
331 *lacz* expression in C4da neurons by DN-Rab11 (**Figure 7A**), which was completely abolished by
332 treating larvae with DLKi/GNE-3511, Wnd kinase inhibitor. This strongly suggests that increased
333 Wnd protein levels, hence Wnd activity mediates JNK activation induced by DN-Rab11.

334 Expressing DN-Rab11 caused severe eye loss phenotypes (**Figure 7B**). To test whether
335 increased Wnd expression contributes to the neuronal loss caused by DN-Rab11, we treated
336 DN-Rab11 expressing flies with Wnd kinase inhibitor, DLKi/GNE-3511. The treatment partially
337 but significantly mitigated eye loss phenotype caused by DN-Rab11 expression (Elav-GAL4/DN-
338 Rab11) while having no effect on eye development in control flies (Elav-GAL4 and DN-Rab11)
339 (**Figure 7B**). Furthermore, genetically reducing Wnd activity by introducing a loss of *wnd* allele,
340 wnd^3, in DN-Rab11 expressing photoreceptors significantly ameliorated the eye loss phenotypes
341 by DN-Rab11 (**Figure 7C**).

342 Taken together, these support a model in which Wnd proteins are transported to the axon
343 terminals for Hiw-mediated protein degradation under normal conditions, and that Rab11 is
344 essential for anterograde sorting of Wnd towards axon terminals. In this model, Rab11
345 inactivation leads to defective anterograde transport of Wnd, thus a deficit in Wnd protein
346 degradation. Subsequent increase in Wnd protein levels triggers excessive stress signaling
347 leading to neuronal death (**Figure 8**).

348

349 Discussion

350 Here, we report that axonal localization and protein turnover of Wnd are tightly coupled and that
351 failure in this coupling leads to dysregulated Wnd protein turnover and triggers excessive stress
352 signaling. We further uncover the role of Rab11 in this coupling.

353 Many neuronal proteins exhibit polarized protein expression patterns. DLK proteins are found in
354 the axonal compartments of diverse animals (Xiong et al., 2010; Klinedinst et al., 2013; Holland
355 et al., 2016; Niu et al., 2020, 2022). However, the extent of DLK axonal localization has not
356 been thoroughly studied, presumably because of technical limitations. We employed *Drosophila*
357 larval sensory neurons to answer this question. Our data suggests that Wnd proteins are highly
358 enriched in the axon terminals of these neurons (**Figure 1**). Given that Wnd encodes a
359 cytoplasmic protein, the extent of axonal enrichment was rather surprising. Wnd protein levels
360 are constantly suppressed by Hiw in the axon terminals. Without such suppression, Wnd
361 proteins would show well over 70-fold enrichment in axons. The UTRs of *wnd* are dispensable
362 for Wnd axonal enrichment (**Figure 1C**), which suggests that axonal anterograde transport of
363 Wnd is responsible for such axonal enrichment. This is supported by previous observations of
364 DLK proteins on membrane vesicles undergoing both anterograde and retrograde transport in
365 axons (Xiong et al., 2010; Holland et al., 2016; Li et al., 2017). Taken together, these indicate
366 that Wnd proteins are synthesized in the neuronal cell body and subsequently transported into
367 axon terminals through a highly active and efficient anterograde transport process.

368 What might be such a transport mechanism? DLK genes encode cytoplasmic proteins. Protein
369 palmitoylation is an important post-translational mechanism for protein transport (Aicart-Ramos
370 et al., 2011; Tortosa and Hoogenraad, 2018). It increases hydrophobicity of target proteins to aid
371 membrane association so that palmitoylated proteins are transported along with the membrane
372 vesicles they associate. In our study, we found that protein palmitoylation on Wnd at the
373 Cysteine residue 130 (Wnd-C130) is essential for its axonal localization. Interestingly, the

374 palmitoylation-defective mutant Wnd-C130S exhibited large punctate structures in the cell body
375 (**Figure 2E**), which colocalized with the somatic Golgi complex (**Figure 2 – supplement 1**). This
376 suggests that Wnd-C130 palmitoylation is not solely responsible for membrane association. The
377 presence of residual palmitoylation in Wnd-C130S (**Figure 2D**) may indicate the existence of an
378 additional palmitoylation site, which may explain how Wnd-C130S associates with the Golgi.
379 Consistent with our findings, previous studies have shown that DLK proteins in mammalian cells
380 and *C. elegans* are palmitoylated on a single Cysteine residue, and when this residue is
381 mutated, the proteins exhibit a diffuse cytoplasmic expression pattern (Holland et al., 2016).
382 These observations raise the question of why Wnd-C130S, with its residual palmitoylation and
383 membrane association, fails to be transported to axon terminals. Interestingly, recent research
384 has proposed a role for protein palmitoylation in anterograde transport within the Golgi complex
385 (Ernst et al., 2018). We envision that Wnd-C130 palmitoylation is a necessary sorting step
386 towards the axonal anterograde transport from the somatic Golgi complex rather than merely
387 acting as a membrane anchor.

388 The role of Rab11 in Wnd axonal targeting and protein turnover uncovered by our DN-Rab
389 screening suggests a role of RE in these processes (**Figure 5 and 6**). Rab11 plays a critical role
390 in membrane trafficking events at the RE and is often used as a marker for the RE (Taguchi,
391 2013). It is involved in the anterograde transport of cargo from the Golgi apparatus to the
392 plasma membrane through the RE (Ang et al., 2004; Satoh et al., 2005; Taguchi, 2013). We
393 envision that once Wnd is palmitoylated, it is sorted at the peri-nuclear RE for subsequent
394 axonal anterograde transport. Our observation of significant colocalization between Wnd
395 proteins and Rab11-positive puncta in C4da cell bodies (**Figure 6**) but not in axon terminals or
396 in axons (**Figure 6 - supplement 1**) supports the idea that Wnd proteins are associated with the
397 RE during their anterograde transport. These further suggest that Rab11 is not directly involved

398 in the anterograde long-distance transport of Wnd proteins, rather is responsible for sorting Wnd
399 into the axonal anterograde transporting vesicles.

400 Inhibiting Rab11 activity led to increased Wnd protein levels (**Figure 6E**). Reduced activity or
401 expression levels of Rab11 have been reported in experimental models of Huntington's disease,
402 Parkinson's disease and in patients with amyotrophic lateral sclerosis (Li et al., 2009a, 2010;
403 Breda et al., 2015; Mitra et al., 2019; Rai and Kumar Roy, 2022). Furthermore, recent studies
404 point to the involvement of DLK in multiple neurodegenerative conditions (Pozniak et al., 2013;
405 Welsbie et al., 2013, 2017; Larhammar et al., 2017a; Le Pichon et al., 2017; Patel et al., 2017).
406 These raise a tantalizing possibility that disrupted anterograde transport of DLK, and
407 subsequent dysregulated DLK protein turnover, could be a contributing factor in these
408 neurodegenerative disorders. In this regard, it is highly encouraging that inhibiting Wnd activity
409 mitigated the neuronal loss and JNK activation by *Rab11* loss-of-function (**Figure 7**). Further
410 investigations are needed to elucidate the causal role of dysregulated DLK protein turnover in
411 neurodegenerative conditions and to better understand the interplay between Rab11-mediated
412 transport, protein turnover, and DLK-mediated stress signaling.

413 The mechanism by which Hiw performs compartmentalized Wnd protein turnover in axons is an
414 interesting question. There are several possibilities to consider. One possibility is that Hiw
415 protein itself is specifically present in the axon terminals and not in the cell body. Studies have
416 shown that Phr1, the mammalian homolog of Hiw, is expressed in axonal segments of motor
417 neuron explants and in the axon shaft of sensory neurons, but its expression in the growth cone
418 is low or absent (Lewcock et al., 2007). However, it is not known whether Hiw proteins are
419 present in the cell body and to what extent. Unfortunately, the lack of an immunostaining
420 compatible Hiw antibody has limited our ability to test this possibility. Nevertheless, transgenic
421 expression of GFP::Hiw in *Drosophila* has shown significantly higher expression in the motor
422 neuron cell bodies (Xiong et al., 2010). Moreover, a study has demonstrated that Hiw controls

423 the expression of dNMNAT2, a substrate of Hiw, both in the cell body and the neuromuscular
424 junction (Xiong et al., 2012). These observations suggest that Hiw expression itself may not be
425 restricted to the axon terminals. Another possibility is that DLK proteins are protected from
426 PHR1/RMP-1/Hiw-mediated protein turnover in the cell body. DLK protein stability can be
427 enhanced by Hsp90 (Karney-Grobe et al., 2018), protein phosphorylation by JNK (Huntwork-
428 Rodriguez et al., 2013), and PKA (Hao et al., 2016). These protective pathways may collaborate
429 with PHR1/RMP-1/Hiw to execute axon-specific protein turnover of DLK proteins.
430 Understanding the interplay between these protective mechanisms and PHR1/RMP-1/Hiw in
431 regulating DLK protein turnover will provide valuable insights on subcellular specific Wnd protein
432 turnover.

433 The coupling between axonal transport and protein turnover of DLK proteins may have
434 important implications in the context of neurodegenerative disorders. Recent studies have
435 implicated DLK as a central player in neuronal death, including in diseases such as Alzheimer's
436 disease and amyotrophic lateral sclerosis (Pozniak et al., 2013; Welsbie et al., 2013, 2017;
437 Larhammar et al., 2017a, 2017b; Le Pichon et al., 2017; Patel et al., 2017). Defective axonal
438 transport is a common feature observed in many neurodegenerative disorders (Chevalier-
439 Larsen and Holzbaur, 2006; De Vos et al., 2008; Guo et al., 2020), and it has been proposed to
440 contribute to disease pathogenesis. Interestingly, studies have reported increased DLK protein
441 levels in neuronal cell bodies following neuronal insults (Watkins et al., 2013; Welsbie et al.,
442 2013). Furthermore, DLK signaling has been shown to be activated by cytoskeletal disruptions
443 (Valakh et al., 2013, 2015), which may impair cytoskeleton-based axonal transport. This raises
444 an intriguing possibility that disrupted axonal transport, leading to the accumulation of DLK
445 proteins, could be a contributing factor for DLK activation and neuronal loss in
446 neurodegenerative diseases.

447

448 Materials and Methods

449 **Drosophila Strains, rearing, DNA Constructs for Generating Transgenic Flies**

450 The following *Drosophila* strains were reared at 25°C in a humidified chamber. *ppk-GAL4*
451 (Grueber et al., 2007); *UAS-dHIP14::Tdtomato* and *Dhip14*^{ex11} (Stowers and Isacoff, 2007);
452 *hiw*$^{\Delta N}$ (Wu et al., 2005); *UAS-ManII::GFP* (Ye et al., 2007); *UAS-ManII-Tag::RFP* (Zhou et al.,
453 2014); *Mi{MIC}wnd* ^{GFSTF} (Venken et al., 2011); *GMR-Gal4* (Seong et al., 2001); *elav-Gal4*^{C155}
454 (BDSC #459); *w*^{1118} (BDSC #3605); *TI{TI}Rab11*^{EYFP} (BDSC #62549)(Dunst et al., 2015); *UASp-*
455 *YFP.Rab11* (BDSC #50782)(Zhang et al., 2007); *Rab11*^{93Bi} (BDSC #4158)(Giansanti et al.,
456 2007); *puc-lacZ* (Martin-Blanco et al., 1998). For DN-Rab screening, the fly lines (Zhang et al.,
457 2007) were obtained from the Bloomington Drosophila Stock Center and the full list of fly lines is
458 provided in Table 1.

459

460 To generate DNA constructs of *Wnd* with its natural 5'- and 3'-UTRs and the serial deletion
461 constructs of Wnd, the genomic sequences of the 5'-UTR and 3'-UTR of *Wnd* were obtained
462 from *w*^{1118} genomic DNA by PCR. The coding sequence of *Wnd* was recovered from UAS-Wnd
463 (Collins et al., 2006) via PCR and inserted into the pUASTattB plasmid using NotI and XbaI
464 restriction sites. UAS-Wnd-KD::GFP, Wnd-KD∆100::GFP, and WndC130S-KD::GFP were
465 generated by site-directed mutagenesis using In-Fusion® Snap Assembly Master Mix (Takara
466 Bio USA, Inc, San Jose, CA). UAS-Wnd-C130S::GFP and UAS-Wnd∆101-200::GFP were
467 generated by site-directed mutagenesis. To generate UAS-Wnd-KD::mRFP, the coding
468 sequence of Wnd-KD was obtained from UAS-Wnd-KD::GFP via PCR and inserted into the
469 pUASTattB plasmid using NotI and XbaI sites. To generate 2XUAS-Wnd::GFP and 2XUAS-Wnd-
470 C130S::GFP, the coding sequences of Wnd and Wnd-C130S were obtained from UAS-
471 Wnd::GFP and UAS-Wnd-C130S::GFP via PCR respectively. Subsequently, they were inserted

472 into the p2xUASTattB plasmid (Addgene #189860)(Singh and Kim, 2022) using NotI and XbaI
473 restriction sites.

474 Transgenic flies were generated by PhiC31-mediated germline transformation using an identical
475 landing site (Bischof et al., 2007).

476 To dose larvae with DLKi (GNE-3511, Sigma Aldrich), DLKi was dissolved in DMSO and was
477 added to a final concentration of 35 μM in fly food. Fly larvae were raised directly on either
478 control (DMSO) or DLKi containing food.

479

480 **Drosophila Schneider 2 cell culture, transfection, Palmitoylation assay, and Western blot.**

481 *Drosophil*a Schneider 2 (S2) cells were prepared as previously described (Singh et al., 2022).
482 Cells were transfected with indicated DNA constructs and tubulin-Gal4 (Lee and Luo, 1999)
483 using polyethyleneimine (Polysciences, Warrington, PA) (Longo et al., 2013).

484 Two days after transfection, the Acyl-Biotin Exchange (ABE) assay was performed (Drisdel et
485 al., 2006). Cells were lysed in the ice-cold Lysis buffer (LB, 50 mM HEPES/pH 7.4, 150 mM
486 NaCl, 1 mM EDTA, 1% NP40, 5% glycerol, 1 mM PMSF, 1 mM Na_3VO_4, 5 mM NaF) with Halt™
487 protease inhibitor cocktail EDTA- free (ThermoFisher Scientific, Waltham, MA) and 25 mM N-
488 ethylmaleimide (Sigma, St. Louis, MO), incubated for 1hr at 4˚C and centrifuged at 1000 xg for 5
489 min. The resulting post-nuclear lysates were centrifuged at 20,000 x g for 30 min at 4˚C. The
490 supernatant was incubated with the GFP selector (NanoTag Biotechnologies, Göttingen,
491 Germany) for 2 hr at 4˚C to pulldown Wnd-GFP proteins. The GFP selector beads along with
492 bound proteins were recovered by a brief centrifugation and washed two times with LB
493 containing 0.1% SDS before incubating with 1 M hydroxylamine hydrochloride (HAM, Sigma, St.
494 Louis, MO) in LB (pH 7.2) at room temperature for 1 hr. Half of the protein-bound GFP selector
495 beads were incubated with LB without HAM and used as a “- HAM” control. Then, the protein

496 GFP selector beads were washed with pH 6.2 LB twice and treated with 1.6 μM EZ-Link™
497 BMCC-Biotin (ThermoFisher Scientific, Waltham, MA) in pH 6.2 LB for 45 min at 4˚C. Beads
498 were washed twice with LB without NP40 before being processed for SDS-PAGE. Proteins were
499 separated by SDS-PAGE and were subjected to Western blot analysis with mouse monoclonal
500 anti-Biotin antibody (Jackson Immunoresearch, West Grove, PA) and chicken polyclonal anti-
501 GFP antibody (Aves Labs, Tigard, OR).

502 To measure Wnd expression in larva brain lysates, larvae were grown on fly food containing 35
503 μM DLKi food in a humidified chamber. The larval central nervous system (the ventral nerve
504 cord and brain lobes) was dissected out from the 3rd instar larvae and collected in ice-cold PBS
505 before recovery by a brief centrifugation at 4°C. The total brain lysates were prepared by directly
506 adding SDS-PAGE sample buffer and homogenization before being resolved on 8% SDS-PAGE
507 gel and subsequent Western blot analysis. The samples were blotted using anti-Wnd antibody
508 (Collins et al., 2006) to estimate total Wnd proteins. Anti-Elav antibody (DSHB - 9F8A9)(O'Neill
509 et al., 1994) was used as a loading control.

510

511 **Immunostaining and Imaging**

512 *Drosophila* 3rd instar larvae were prepared for immunostaining as previously described (Singh et
513 al., 2022). Primary antibodies used were rabbit polyclonal anti-RFP (Rockland
514 Immunochemicals, Limerick, PA), chicken polyclonal anti-GFP (Aves Labs, Tigard, OR), and
515 goat anti-horseradish peroxidase conjugated with Cy5 (Jackson ImmunoResearch, West Grove,
516 PA). The secondary antibodies used were Cy2- or Cy5-conjugated goat anti-chicken and Cy2-
517 or Cy5-conjugated goat anti-Rabbit (Jackson ImmunoResearch, West Grove, PA).

518 Confocal imaging was done with a Leica SP8 confocal system, or a custom-built spinning disk
519 confocal microscope equipped with a 63x oil-immersion objective with a 0.3 μm step-sizes.

520 For Wnd axonal enrichment analysis, the C4da neuron cell bodies from abdominal segments 4-
521 6 and the corresponding segments in the ventral nerve cord were imaged. The resulting 3D
522 images were projected into 2D images using a maximum projection method in the imageJ
523 software. A region of interest was drawn in the cell body of C4da neurons, and the mean
524 fluorescence intensity was measured using ImageJ software. The mean fluorescence intensity
525 of UAS-mCD8::mRFP transgene expression was measured from the same region of interest
526 and used as a normalization control. The mean intensities of the C4da cell bodies from a single
527 larva were averaged out to calculate the axonal enrichment index. The axonal enrichment index
528 was defined as Wnd expression (mean intensity) in the axon terminals divided by an average
529 Wnd expression in cell bodies (mean intensity).

530 To analyze Golgi and Wnd colocalization, the resulting 3D images were projected into 2D
531 images using a maximum projection method in the ImageJ software. The Manders' Overlap
532 Coefficient (Pike et al., 2017) was measured as the percentage of total GFP signal overlapping
533 with RFP signal using the ImageJ plugin, JACoP (Bolte and Cordelières, 2006). To analyze
534 puncta colocalization, we used the Manders' coefficient (Pike et al., 2017) that is correlation
535 between each channel signal using JACop. For Wnd colocalization with TI-YFP::Rab11, a single
536 confocal slice was selected.

537

538 **Drosophila eye degeneration**

539 The flies that are 24 – 48 hr after eclosion were imaged using the Basler ace acA2440-75 μm
540 CCD-camera or Moticam A5 camera installed on a stereomicroscope. The region of interest was
541 drawn on the fly eye area from the images and expressed as pixel numbers divided by 1000.
542 Flies were raised at 27°C in a humidified incubator except for Figure 4 – supplement 2.

543

544 **Drosophila Viability and Lethality Analysis**

545 Flies were raised at 27°C. Viability was determined by counting the number of filial pupae
546 generation (adult flies after eclosion) and pupae lethality by counting the number of dead pupae
547 per vial.

548

549 **Quantitative reverse transcription PCR**

550 Total RNAs were extracted from the wondering third instar larval brains from a wild-type (w^{1118})
551 or homozygous *Rab11* ^{93bi} mutants using the Quick-RNA MicroPrep kit (Zymo Research, Irvine,
552 CA), and were subjected to reverse transcription using a mixture of gene-specific primers as
553 follows, GAPDH1 (CTTCATTCGATGCACAAGTTTTATTTTTCAAATAGCTGG) and wnd
554 (CCATACAGTTTAGGTCGATTTCTC, CAACTTCGGGCCTAATCAAGG,
555 GCGTAACTTGGACAACTCCAA, GGAGATAGTTTTTGCTGCGTAAC, and
556 GGCCCCCACCTAGACTAGAT).

557 The quantitative PCR was conducted using SYBR MasterMix (ThermoFisher Scientific,
558 Waltham, MA). The following gene specific primer pairs were used.

559 GAPDH1, ATGTCTCCGTTGTGGATCTTAC and CCTCGACCTTAGCCTTGATTT; wnd primer1,
560 TCTGCGGAGAAGAAGCATTGG and TGGATGGCAATCTTCTGGGAG; wnd primer 2,
561 GTTCGATAGGCAATGCCAAC and CGCAGAGCGTACTTGTAGTC.

562 The mRNA abundance of *wnd* was calculated by the 2ΔΔCT method using GAPDH1 as a
563 normalizing control.

564

565 **Experimental design and statistical analysis.**

566 All statistical analysis was performed as two-tailed using GraphPad Prism software version
567 7.04. The Mann–Whitney test was used for immunostaining results. A ratio paired t-test was
568 used for Western blot analysis (Figure 3A and 6E). For multigroup comparisons, one-way
569 ANOVA was used followed by post hoc Tukey's multiple comparisons tests. The Chi-square test
570 was performed for Drosophila lethality analysis (Figure 4B). A p-value smaller than 0.05 was
571 considered statistically significant. All p values are indicated as NS; non-significant, *; $P < 0.05$,
572 **; $P < 0.01$, ***; $P < 0.001$, and ****; $P < 0.0001$

573

Acknowledgments

We thank Drs. Steve Stowers and Catherine Collins for sharing reagents. Research reported in this study used the Cellular and Molecular Imaging Core facility at the University of Nevada Reno, which was supported by NIH P30 GM145646. This study was supported by NIH R01NS116463 and P20GM103440 (NV INBRE) to J.K. The content is solely the responsibility of the authors and does not necessarily represent the official views of the National Institutes of Health.

Author contributions

S.K., Y.Q., M.S., and J.K. designed the experiments. S.K., Y.Q., and M.S. experiments. S.K. and J.K. wrote the manuscript.

Declaration of interests

The authors declare no competing financial interests.

588 References

589 Aicart-Ramos, C., Valero, R.A., and Rodriguez-Crespo, I. (2011). Protein palmitoylation and
590 subcellular trafficking. Biochim Biophys Acta 1808, 2981-2994. 10.1016/j.bbamem.2011.07.009.

591 Ang, A.L., Taguchi, T., Francis, S., Fölsch, H., Murrells, L.J., Pypaert, M., Warren, G., and
592 Mellman, I. (2004). Recycling endosomes can serve as intermediates during transport from the
593 Golgi to the plasma membrane of MDCK cells. J Cell Biol 167, 531-543.
594 10.1083/jcb.200408165.

595 Bischof, J., Maeda, R.K., Hediger, M., Karch, F., and Basler, K. (2007). An optimized
596 transgenesis system for Drosophila using germ-line-specific phiC31 integrases. Proc Natl Acad
597 Sci U S A 104, 3312-3317. 10.1073/pnas.0611511104.

598 Bolte, S., and Cordelières, F.P. (2006). A guided tour into subcellular colocalization analysis in
599 light microscopy. J Microsc 224, 213-232. 10.1111/j.1365-2818.2006.01706.x.

600 Breda, C., Nugent, M.L., Estranero, J.G., Kyriacou, C.P., Outeiro, T.F., Steinert, J.R., and
601 Giorgini, F. (2015). Rab11 modulates α-synuclein-mediated defects in synaptic transmission and
602 behaviour. Hum Mol Genet 24, 1077-1091. 10.1093/hmg/ddu521.

603 Calkins, M.J., Manczak, M., Mao, P., Shirendeb, U., and Reddy, P.H. (2011). Impaired
604 mitochondrial biogenesis, defective axonal transport of mitochondria, abnormal mitochondrial
605 dynamics and synaptic degeneration in a mouse model of Alzheimer's disease. Hum Mol Genet
606 20, 4515-4529. 10.1093/hmg/ddr381.

607 Chevalier-Larsen, E., and Holzbaur, E.L. (2006). Axonal transport and neurodegenerative
608 disease. Biochim Biophys Acta 1762, 1094-1108. 10.1016/j.bbadis.2006.04.002.

609 Chu, Y., Morfini, G.A., Langhamer, L.B., He, Y., Brady, S.T., and Kordower, J.H. (2012).
610 Alterations in axonal transport motor proteins in sporadic and experimental Parkinson's disease.
611 Brain 135, 2058-2073. 10.1093/brain/aws133.

612 Collard, J.F., Côté, F., and Julien, J.P. (1995). Defective axonal transport in a transgenic mouse
613 model of amyotrophic lateral sclerosis. Nature 375, 61-64. 10.1038/375061a0.

614 Collins, C.A., Wairkar, Y.P., Johnson, S.L., and DiAntonio, A. (2006). Highwire restrains synaptic
615 growth by attenuating a MAP kinase signal. Neuron 51, 57-69. 10.1016/j.neuron.2006.05.026.

616 De Vos, K.J., Grierson, A.J., Ackerley, S., and Miller, C.C. (2008). Role of axonal transport in
617 neurodegenerative diseases. Annu Rev Neurosci 31, 151-173.
618 10.1146/annurev.neuro.31.061307.090711.

619 De Vos, K.J., and Hafezparast, M. (2017). Neurobiology of axonal transport defects in motor
620 neuron diseases: Opportunities for translational research? Neurobiol Dis 105, 283-299.
621 10.1016/j.nbd.2017.02.004.

622 Dunst, S., Kazimiers, T., von Zadow, F., Jambor, H., Sagner, A., Brankatschk, B., Mahmoud, A.,
623 Spannl, S., Tomancak, P., Eaton, S., and Brankatschk, M. (2015). Endogenously tagged rab
624 proteins: a resource to study membrane trafficking in Drosophila. Dev Cell 33, 351-365.
625 10.1016/j.devcel.2015.03.022.

626 Drisdel, R.C., Alexander, J.K., Sayeed, A., and Green, W.N. (2006). Assays of protein
627 palmitoylation. Methods 40, 127-134. 10.1016/j.ymeth.2006.04.015.

628 Ernst, A.M., Syed, S.A., Zaki, O., Bottanelli, F., Zheng, H., Hacke, M., Xi, Z., Rivera-Molina, F.,
629 Graham, M., Rebane, A.A., et al. (2018). S-Palmitoylation Sorts Membrane Cargo for
630 Anterograde Transport in the Golgi. Dev Cell 47, 479-493.e477. 10.1016/j.devcel.2018.10.024.

631 Ghosh, A.S., Wang, B., Pozniak, C.D., Chen, M., Watts, R.J., and Lewcock, J.W. (2011). DLK
632 induces developmental neuronal degeneration via selective regulation of proapoptotic JNK
633 activity. J Cell Biol 194, 751-764. 10.1083/jcb.201103153.

634 Giansanti, M.G., Belloni, G., and Gatti, M. (2007). Rab11 is required for membrane trafficking
635 and actomyosin ring constriction in meiotic cytokinesis of Drosophila males. Mol Biol Cell 18,
636 5034-5047. 10.1091/mbc.e07-05-0415.

637 Grueber, W.B., Ye, B., Yang, C.H., Younger, S., Borden, K., Jan, L.Y., and Jan, Y.N. (2007).
638 Projections of Drosophila multidendritic neurons in the central nervous system: links with
639 peripheral dendrite morphology. Development 134, 55-64. 10.1242/dev.02666.

640 Guedes-Dias, P., and Holzbaur, E.L.F. (2019). Axonal transport: Driving synaptic function.
641 Science 366. 10.1126/science.aaw9997.

642 Guillaud, L., El-Agamy, S.E., Otsuki, M., and Terenzio, M. (2020). Anterograde Axonal Transport
643 in Neuronal Homeostasis and Disease. Front Mol Neurosci 13, 556175.
644 10.3389/fnmol.2020.556175.

645 Guo, W., Stoklund Dittlau, K., and Van Den Bosch, L. (2020). Axonal transport defects and
646 neurodegeneration: Molecular mechanisms and therapeutic implications. Semin Cell Dev Biol
647 99, 133-150. 10.1016/j.semcdb.2019.07.010.

648 Hao, Y., Frey, E., Yoon, C., Wong, H., Nestorovski, D., Holzman, L.B., Giger, R.J., DiAntonio, A.,
649 and Collins, C. (2016). An evolutionarily conserved mechanism for cAMP elicited axonal
650 regeneration involves direct activation of the dual leucine zipper kinase DLK. Elife 5.
651 10.7554/eLife.14048.

652 Holland, S.M., Collura, K.M., Ketschek, A., Noma, K., Ferguson, T.A., Jin, Y., Gallo, G., and
653 Thomas, G.M. (2016). Palmitoylation controls DLK localization, interactions and activity to
654 ensure effective axonal injury signaling. Proc Natl Acad Sci U S A 113, 763-768.
655 10.1073/pnas.1514123113.

656 Huntwork-Rodriguez, S., Wang, B., Watkins, T., Ghosh, A.S., Pozniak, C.D., Bustos, D.,
657 Newton, K., Kirkpatrick, D.S., and Lewcock, J.W. (2013). JNK-mediated phosphorylation of DLK
658 suppresses its ubiquitination to promote neuronal apoptosis. J Cell Biol 202, 747-763.
659 10.1083/jcb.201303066.

660 Karney-Grobe, S., Russo, A., Frey, E., Milbrandt, J., and DiAntonio, A. (2018). HSP90 is a
661 chaperone for DLK and is required for axon injury signaling. Proc Natl Acad Sci U S A 115,
662 E9899-E9908. 10.1073/pnas.1805351115.

663 Klinedinst, S., Wang, X., Xiong, X., Haenfler, J.M., and Collins, C.A. (2013). Independent
664 pathways downstream of the Wnd/DLK MAPKKK regulate synaptic structure, axonal transport,
665 and injury signaling. J Neurosci 33, 12764-12778. 10.1523/JNEUROSCI.5160-12.2013.

666 Larhammar, M., Huntwork-Rodriguez, S., Jiang, Z., Solanoy, H., Sengupta Ghosh, A., Wang, B.,
667 Kaminker, J.S., Huang, K., Eastham-Anderson, J., Siu, M., et al. (2017). Dual leucine zipper
668 kinase-dependent PERK activation contributes to neuronal degeneration following insult. Elife 6.
669 10.7554/eLife.20725.

670 Larhammar, M., Huntwork-Rodriguez, S., Rudhard, Y., Sengupta-Ghosh, A., and Lewcock, J.W.
671 (2017). The Ste20 Family Kinases MAP4K4, MINK1, and TNIK Converge to Regulate Stress-
672 Induced JNK Signaling in Neurons. J Neurosci 37, 11074-11084. 10.1523/JNEUROSCI.0905-
673 17.2017.

674 Le Pichon, C.E., Meilandt, W.J., Dominguez, S., Solanoy, H., Lin, H., Ngu, H., Gogineni, A.,
675 Sengupta Ghosh, A., Jiang, Z., Lee, S.H., et al. (2017). Loss of dual leucine zipper kinase
676 signaling is protective in animal models of neurodegenerative disease. Sci Transl Med 9.
677 10.1126/scitranslmed.aag0394.

678 Lee, T., and Luo, L. (1999). Mosaic analysis with a repressible cell marker for studies of gene
679 function in neuronal morphogenesis. Neuron 22, 451-461. 10.1016/s0896-6273(00)80701-1.

680 Lee, W.C., Yoshihara, M., and Littleton, J.T. (2004). Cytoplasmic aggregates trap polyglutamine-
681 containing proteins and block axonal transport in a Drosophila model of Huntington's disease.
682 Proc Natl Acad Sci U S A 101, 3224-3229. 10.1073/pnas.0400243101.

683 Lewcock, J.W., Genoud, N., Lettieri, K., and Pfaff, S.L. (2007). The ubiquitin ligase Phr1
684 regulates axon outgrowth through modulation of microtubule dynamics. Neuron 56, 604-620.
685 10.1016/j.neuron.2007.09.009.

686 Li, J., Zhang, Y.V., Asghari Adib, E., Stanchev, D.T., Xiong, X., Klinedinst, S., Soppina, P., Jahn,
687 T.R., Hume, R.I., Rasse, T.M., and Collins, C.A. (2017). Restraint of presynaptic protein levels
688 by Wnd/DLK signaling mediates synaptic defects associated with the kinesin-3 motor Unc-104.
689 Elife 6. 10.7554/eLife.24271.

690 Li, X., Sapp, E., Chase, K., Comer-Tierney, L.A., Masso, N., Alexander, J., Reeves, P., Kegel,
691 K.B., Valencia, A., Esteves, M., et al. (2009). Disruption of Rab11 activity in a knock-in mouse
692 model of Huntington's disease. Neurobiol Dis 36, 374-383. 10.1016/j.nbd.2009.08.003.

693 Li, X., Standley, C., Sapp, E., Valencia, A., Qin, Z.H., Kegel, K.B., Yoder, J., Comer-Tierney,
694 L.A., Esteves, M., Chase, K., et al. (2009). Mutant huntingtin impairs vesicle formation from
695 recycling endosomes by interfering with Rab11 activity. Mol Cell Biol 29, 6106-6116.
696 10.1128/MCB.00420-09.

697 Li, X., Valencia, A., Sapp, E., Masso, N., Alexander, J., Reeves, P., Kegel, K.B., Aronin, N., and
698 Difiglia, M. (2010). Aberrant Rab11-dependent trafficking of the neuronal glutamate transporter
699 EAAC1 causes oxidative stress and cell death in Huntington's disease. J Neurosci 30, 4552-
700 4561. 10.1523/JNEUROSCI.5865-09.2010.

701 Li, Y., Ritchie, E.M., Steinke, C.L., Qi, C., Chen, L., Zheng, B., and Jin, Y. (2021). Activation of
702 MAP3K DLK and LZK in Purkinje cells causes rapid and slow degeneration depending on
703 signaling strength. Elife 10. 10.7554/eLife.63509.

704 Longo, P.A., Kavran, J.M., Kim, M.S., and Leahy, D.J. (2013). Transient mammalian cell
705 transfection with polyethylenimine (PEI). Methods Enzymol 529, 227-240. 10.1016/B978-0-12-
706 418687-3.00018-5.

707 Martin, D.D.O., Kanuparthi, P.S., Holland, S.M., Sanders, S.S., Jeong, H.K., Einarson, M.B.,
708 Jacobson, M.A., and Thomas, G.M. (2019). Identification of Novel Inhibitors of DLK
709 Palmitoylation and Signaling by High Content Screening. Sci Rep 9, 3632. 10.1038/s41598-019-
710 39968-8.

711 Martín-Blanco, E., Gampel, A., Ring, J., Virdee, K., Kirov, N., Tolkovsky, A.M., and Martinez-
712 Arias, A. (1998). puckered encodes a phosphatase that mediates a feedback loop regulating
713 JNK activity during dorsal closure in Drosophila. Genes Dev 12, 557-570.
714 10.1101/gad.12.4.557.

715 Miller, B.R., Press, C., Daniels, R.W., Sasaki, Y., Milbrandt, J., and DiAntonio, A. (2009). A dual
716 leucine kinase-dependent axon self-destruction program promotes Wallerian degeneration. Nat
717 Neurosci 12, 387-389. 10.1038/nn.2290.

718 Mitra, J., Hegde, P.M., and Hegde, M.L. (2019). Loss of endosomal recycling factor RAB11
719 coupled with complex regulation of MAPK/ERK/AKT signaling in postmortem spinal cord
720 specimens of sporadic amyotrophic lateral sclerosis patients. Mol Brain 12, 55. 10.1186/s13041-
721 019-0475-y.

722 Nakata, K., Abrams, B., Grill, B., Goncharov, A., Huang, X., Chisholm, A.D., and Jin, Y. (2005).
723 Regulation of a DLK-1 and p38 MAP kinase pathway by the ubiquitin ligase RPM-1 is required
724 for presynaptic development. Cell 120, 407-420. 10.1016/j.cell.2004.12.017.

725 Niu, J., Holland, S.M., Ketschek, A., Collura, K.M., Hesketh, N.L., Hayashi, T., Gallo, G., and
726 Thomas, G.M. (2022). Palmitoylation couples the kinases DLK and JNK3 to facilitate
727 prodegenerative axon-to-soma signaling. Sci Signal 15, eabh2674. 10.1126/scisignal.abh2674.

728 Niu, J., Sanders, S.S., Jeong, H.K., Holland, S.M., Sun, Y., Collura, K.M., Hernandez, L.M.,
729 Huang, H., Hayden, M.R., Smith, G.M., et al. (2020). Coupled Control of Distal Axon Integrity
730 and Somal Responses to Axonal Damage by the Palmitoyl Acyltransferase ZDHHC17. Cell Rep
731 33, 108365. 10.1016/j.celrep.2020.108365.

732 Patel, S., Meilandt, W.J., Erickson, R.I., Chen, J., Deshmukh, G., Estrada, A.A., Fuji, R.N.,
733 Gibbons, P., Gustafson, A., Harris, S.F., et al. (2017). Selective Inhibitors of Dual Leucine Zipper
734 Kinase (DLK, MAP3K12) with Activity in a Model of Alzheimer's Disease. J Med Chem 60, 8083-
735 8102. 10.1021/acs.jmedchem.7b00843.

736 Pensalfini, A., Kim, S., Subbanna, S., Bleiwas, C., Goulbourne, C.N., Stavrides, P.H., Jiang, Y.,
737 Lee, J.H., Darji, S., Pawlik, M., et al. (2020). Endosomal Dysfunction Induced by Directly
738 Overactivating Rab5 Recapitulates Prodromal and Neurodegenerative Features of Alzheimer's
739 Disease. Cell Rep 33, 108420. 10.1016/j.celrep.2020.108420.

740 Pike, J.A., Styles, I.B., Rappoport, J.Z., and Heath, J.K. (2017). Quantifying receptor trafficking
741 and colocalization with confocal microscopy. Methods 115, 42-54. 10.1016/j.ymeth.2017.01.005.

742 Pozniak, C.D., Sengupta Ghosh, A., Gogineni, A., Hanson, J.E., Lee, S.H., Larson, J.L.,
743 Solanoy, H., Bustos, D., Li, H., Ngu, H., et al. (2013). Dual leucine zipper kinase is required for
744 excitotoxicity-induced neuronal degeneration. J Exp Med 210, 2553-2567.
745 10.1084/jem.20122832.

Rai, P., and Kumar Roy, J. (2022). Endosomal recycling protein Rab11 in Parkin and Pink1 signaling in Drosophila model of Parkinson's disease. Exp Cell Res 420, 113357. 10.1016/j.yexcr.2022.113357.

Reddy, P.H., and Shirendeb, U.P. (2012). Mutant huntingtin, abnormal mitochondrial dynamics, defective axonal transport of mitochondria, and selective synaptic degeneration in Huntington's disease. Biochim Biophys Acta 1822, 101-110. 10.1016/j.bbadis.2011.10.016.

Russo, A., and DiAntonio, A. (2019). Wnd/DLK Is a Critical Target of FMRP Responsible for Neurodevelopmental and Behavior Defects in the Drosophila Model of Fragile X Syndrome. Cell Rep 28, 2581-2593.e2585. 10.1016/j.celrep.2019.08.001.

Saha, A.R., Hill, J., Utton, M.A., Asuni, A.A., Ackerley, S., Grierson, A.J., Miller, C.C., Davies, A.M., Buchman, V.L., Anderton, B.H., and Hanger, D.P. (2004). Parkinson's disease alpha-synuclein mutations exhibit defective axonal transport in cultured neurons. J Cell Sci 117, 1017-1024. 10.1242/jcs.00967.

Satoh, A.K., O'Tousa, J.E., Ozaki, K., and Ready, D.F. (2005). Rab11 mediates post-Golgi trafficking of rhodopsin to the photosensitive apical membrane of Drosophila photoreceptors. Development 132, 1487-1497. 10.1242/dev.01704.

Seong, K.H., Matsuo, T., Fuyama, Y., and Aigaki, T. (2001). Neural-specific overexpression of drosophila plenty of SH3s (DPOSH) extends the longevity of adult flies. Biogerontology 2, 271-281. 10.1023/a:1013249326285.

Shin, J.E., Cho, Y., Beirowski, B., Milbrandt, J., Cavalli, V., and DiAntonio, A. (2012). Dual leucine zipper kinase is required for retrograde injury signaling and axonal regeneration. Neuron 74, 1015-1022. 10.1016/j.neuron.2012.04.028.

Singh, M., and Kim, J.H. (2022). Generation and validation of pX-UASTattB for dose-dependent misexpression studies in. MicroPubl Biol 2022. 10.17912/micropub.biology.000626.

Singh, M., Ye, B., and Kim, J.H. (2022). Dual Leucine Zipper Kinase Regulates Dscam Expression through a Noncanonical Function of the Cytoplasmic Poly(A)-Binding Protein. J Neurosci 42, 6007-6019. 10.1523/JNEUROSCI.0543-21.2022.

Smith, G.A., Rocha, E.M., McLean, J.R., Hayes, M.A., Izen, S.C., Isacson, O., and Hallett, P.J. (2014). Progressive axonal transport and synaptic protein changes correlate with behavioral and neuropathological abnormalities in the heterozygous Q175 KI mouse model of Huntington's disease. Hum Mol Genet 23, 4510-4527. 10.1093/hmg/ddu166.

Stenmark, H. (2009). Rab GTPases as coordinators of vesicle traffic. Nat Rev Mol Cell Biol 10, 513-525. 10.1038/nrm2728.

Stowers, R.S., and Isacoff, E.Y. (2007). Drosophila huntingtin-interacting protein 14 is a presynaptic protein required for photoreceptor synaptic transmission and expression of the palmitoylated proteins synaptosome-associated protein 25 and cysteine string protein. J Neurosci 27, 12874-12883. 10.1523/JNEUROSCI.2464-07.2007.

Taguchi, T. (2013). Emerging roles of recycling endosomes. J Biochem 153, 505-510. 10.1093/jb/mvt034.

785 Tiwari, A.K., and Roy, J.K. (2009). Mutation in Rab11 results in abnormal organization of
786 ommatidial cells and activation of JNK signaling in the Drosophila eye. Eur J Cell Biol 88, 445-
787 460. 10.1016/j.ejcb.2009.02.188.

788 Tortosa, E., and Hoogenraad, C.C. (2018). Polarized trafficking: the palmitoylation cycle
789 distributes cytoplasmic proteins to distinct neuronal compartments. Curr Opin Cell Biol 50, 64-
790 71. 10.1016/j.ceb.2018.02.004.

791 Tortosa, E., Sengupta Ghosh, A., Li, Q., Wong, W.R., Hinkle, T., Sandoval, W., Rose, C.M., and
792 Hoogenraad, C.C. (2022). Stress-induced vesicular assemblies of dual leucine zipper kinase
793 are signaling hubs involved in kinase activation and neurodegeneration. EMBO J 41, e110155.
794 10.15252/embj.2021110155.

795 Valakh, V., Frey, E., Babetto, E., Walker, L.J., and DiAntonio, A. (2015). Cytoskeletal disruption
796 activates the DLK/JNK pathway, which promotes axonal regeneration and mimics a
797 preconditioning injury. Neurobiol Dis 77, 13-25. 10.1016/j.nbd.2015.02.014.

798 Valakh, V., Walker, L.J., Skeath, J.B., and DiAntonio, A. (2013). Loss of the spectraplakin short
799 stop activates the DLK injury response pathway in Drosophila. J Neurosci 33, 17863-17873.
800 10.1523/JNEUROSCI.2196-13.2013.

801 Venken, K.J., Schulze, K.L., Haelterman, N.A., Pan, H., He, Y., Evans-Holm, M., Carlson, J.W.,
802 Levis, R.W., Spradling, A.C., Hoskins, R.A., and Bellen, H.J. (2011). MiMIC: a highly versatile
803 transposon insertion resource for engineering Drosophila melanogaster genes. Nat Methods 8,
804 737-743. 10.1038/nmeth.1662.

805 Wang, X., Kim, J.H., Bazzi, M., Robinson, S., Collins, C.A., and Ye, B. (2013). Bimodal control of
806 dendritic and axonal growth by the dual leucine zipper kinase pathway. PLoS Biol 11, e1001572.
807 10.1371/journal.pbio.1001572.

808 Wang, Z.X., Tan, L., and Yu, J.T. (2015). Axonal transport defects in Alzheimer's disease. Mol
809 Neurobiol 51, 1309-1321. 10.1007/s12035-014-8810-x.

810 Watkins, T.A., Wang, B., Huntwork-Rodriguez, S., Yang, J., Jiang, Z., Eastham-Anderson, J.,
811 Modrusan, Z., Kaminker, J.S., Tessier-Lavigne, M., and Lewcock, J.W. (2013). DLK initiates a
812 transcriptional program that couples apoptotic and regenerative responses to axonal injury. Proc
813 Natl Acad Sci U S A 110, 4039-4044. 10.1073/pnas.1211074110.

814 Welsbie, D.S., Yang, Z., Ge, Y., Mitchell, K.L., Zhou, X., Martin, S.E., Berlinicke, C.A., Hackler,
815 L., Fuller, J., Fu, J., et al. (2013). Functional genomic screening identifies dual leucine zipper
816 kinase as a key mediator of retinal ganglion cell death. Proc Natl Acad Sci U S A 110, 4045-
817 4050. 10.1073/pnas.1211284110.

818 Welsbie, D.S., Mitchell, K.L., Jaskula-Ranga, V., Sluch, V.M., Yang, Z., Kim, J., Buehler, E.,
819 Patel, A., Martin, S.E., Zhang, P.W., et al. (2017). Enhanced Functional Genomic Screening
820 Identifies Novel Mediators of Dual Leucine Zipper Kinase-Dependent Injury Signaling in
821 Neurons. Neuron 94, 1142-1154.e1146. 10.1016/j.neuron.2017.06.008.

822 Wu, C., Wairkar, Y.P., Collins, C.A., and DiAntonio, A. (2005). Highwire function at the
823 Drosophila neuromuscular junction: spatial, structural, and temporal requirements. J Neurosci
824 25, 9557-9566. 10.1523/JNEUROSCI.2532-05.2005.

825 Xiong, X., and Collins, C.A. (2012). A conditioning lesion protects axons from degeneration via
826 the Wallenda/DLK MAP kinase signaling cascade. J Neurosci 32, 610-615.
827 10.1523/JNEUROSCI.3586-11.2012.

828 Xiong, X., Hao, Y., Sun, K., Li, J., Li, X., Mishra, B., Soppina, P., Wu, C., Hume, R.I., and Collins,
829 C.A. (2012). The Highwire ubiquitin ligase promotes axonal degeneration by tuning levels of
830 Nmnat protein. PLoS Biol 10, e1001440. 10.1371/journal.pbio.1001440.

831 Xiong, X., Wang, X., Ewanek, R., Bhat, P., Diantonio, A., and Collins, C.A. (2010). Protein
832 turnover of the Wallenda/DLK kinase regulates a retrograde response to axonal injury. J Cell
833 Biol 191, 211-223. 10.1083/jcb.201006039.

834 Ye, B., Zhang, Y., Song, W., Younger, S.H., Jan, L.Y., and Jan, Y.N. (2007). Growing dendrites
835 and axons differ in their reliance on the secretory pathway. Cell 130, 717-729.
836 10.1016/j.cell.2007.06.032.

837 Zhang, J., Schulze, K.L., Hiesinger, P.R., Suyama, K., Wang, S., Fish, M., Acar, M., Hoskins,
838 R.A., Bellen, H.J., and Scott, M.P. (2007). Thirty-one flavors of Drosophila rab proteins. Genetics
839 176, 1307-1322. 10.1534/genetics.106.066761.

840 Zhou, W., Chang, J., Wang, X., Savelieff, M.G., Zhao, Y., Ke, S., and Ye, B. (2014). GM130 is
841 required for compartmental organization of dendritic golgi outposts. Curr Biol 24, 1227-1233.
842 10.1016/j.cub.2014.04.008.

Figure 1

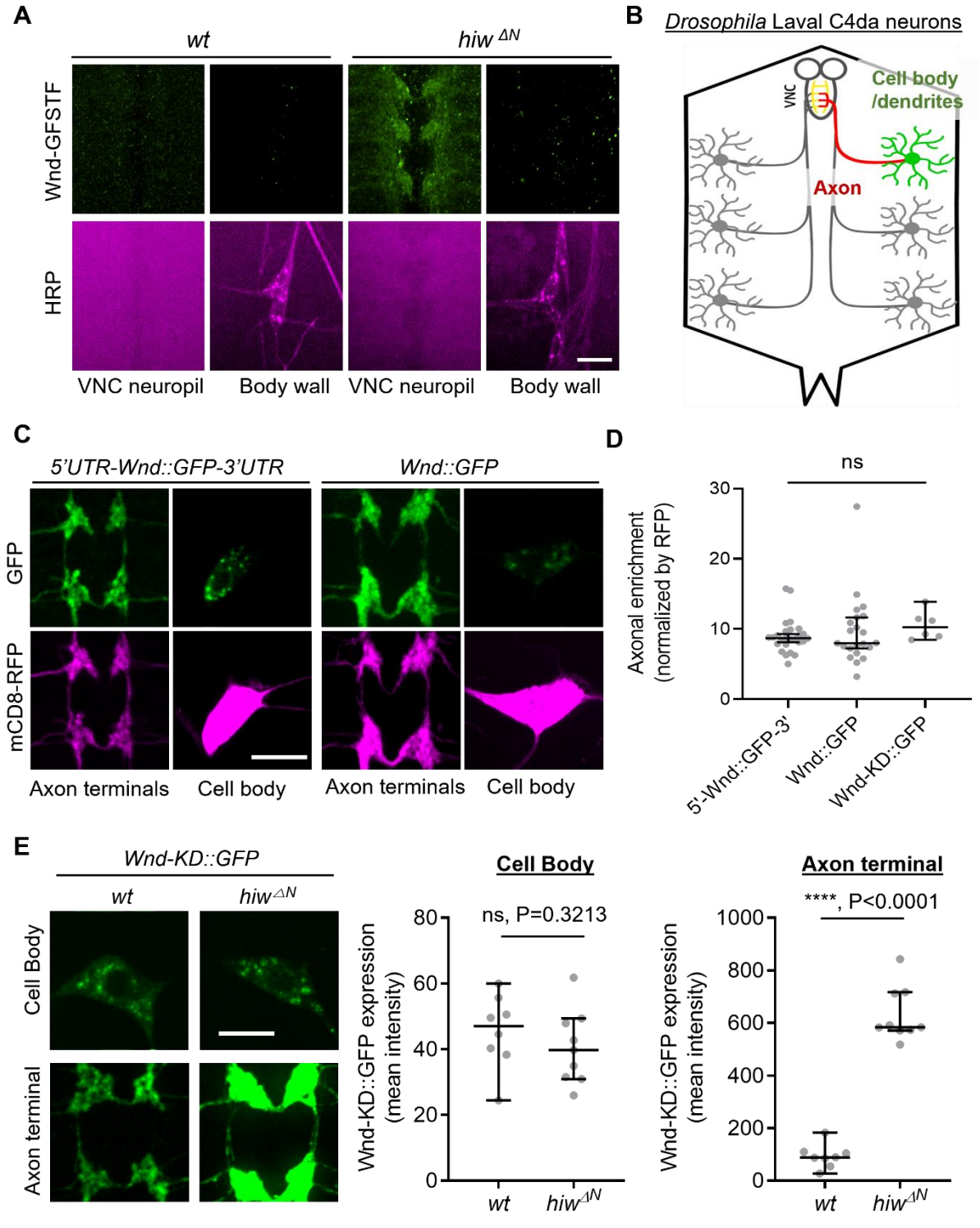
A
wt
hiw ΔN
Wnd-GFSTF
HRP
VNC neuropil
Body wall
VNC neuropil
Body wall
B
Drosophila Laval C4da neurons
VNC
Cell body /dendrites
Axon
C
5'UTR-Wnd::GFP-3'UTR
Wnd::GFP
GFP
mCD8-RFP
Axon terminals
Cell body
Axon terminals
Cell body
D
ns
Axonal enrichment (normalized by RFP)
30
20
10
0
5'-Wnd::GFP-3'
Wnd::GFP
Wnd-KD::GFP
E
Wnd-KD::GFP
wt
hiwΔN
Cell Body
Axon terminal
Cell Body
ns, P=0.3213
Wnd-KD::GFP expression (mean intensity)
80
60
40
20
0
wt
hiwΔN
Axon terminal
****, P<0.0001
Wnd-KD::GFP expression (mean intensity)
1000
800
600
400
200
0
wt
hiwΔN

Fig 1. Wnd protein turnover by Hiw is restricted in the axon terminals of *Drosophila* sensory neurons.

Wnd is highly enriched in axon terminals (A-D).

(A) A representative image of *Mi{MIC}wnd* ^{GFSTF} in the neuropil of larval ventral nerve cords (top) and C4da neuron cell body (bottom) from wild-type male (w^{1118}) or hemizygous male *hiw* mutant ($hiw^{\Delta N}$) were shown. Wnd-GFP (Wnd-GFSTF, green) and anti-HRP staining (magenta). Scale bar = 10 μm.

(B) Schematic of *Drosophila* larval C4da neurons. C4da cell bodies and dendrites are located in the body wall (green) while their axons (red) terminate in the ventral nerve cord (VNC) collectively forming the ladder-like structure of axon terminals (yellow).

(C) The Wnd::GFP (with or without *wnd*-UTRs, green) along with mCD8::RFP (magenta) were expressed in the larval C4da neurons in the presence of DLK inhibitor, DLKi. The expression levels of transgenes were shown in C4da cell body and the axon terminals.

(D) The axonal enrichment index was expressed as median ± 95% CI. Sample numbers were 5'-Wnd::GFP-3' (w^{1118}*; UAS-wnd-5'UTR-Wnd::GFP-wnd-3'UTR/+;ppk-GAL4, UAS-mCD8::RFP/+*) (n = 26), Wnd::GFP (w^{1118}*; UAS-Wnd::GFP-SV40 3'UTR /+; ppk-GAL4, UAS-mCD8::RFP/+*) (n = 22), Wnd-KD::GFP (w^{1118}*; UAS-Wnd-KD::GFP/+; ppk-GAL4, UAS-mCD8::RFP/+*) (n = 6). All samples were treated with DLKi ; One-way ANOVA ($F_{(2,51)} = 0.5176$) followed by post hoc Tukey's multiple comparison test.

(E) The Wnd-KD::GFP transgene along with mCD8::RFP was expressed in C4da neurons with the *ppk-Gal4* driver, in wild-type (*wt*) (w^{1118}*;UAS-Wnd-KD::GFP/+;ppk-Gal4, UAS-mCD8::RFP/+,* sample n = 8) or in *hiw* mutant ($hiw^{\Delta N}$*; UAS-Wnd-KD::GFP/+;ppk-Gal4,UAS-mCD8::RFP/+,* sample n = 9) larvae. Representative images of Wnd-KD::GFP in C4da cell bodies and axon terminals, stained for anti-GFP (green). The average Wnd-KD::GFP intensity from cell bodies and axon terminals were quantified and expressed as median ± 95% CI; (Cell body: U=25, P=0.3213, Axon terminal: U=0, P<0.0001, two-tailed Mann-Whitney test). Scale bar = 10 μm.

Figure 1 - supplement

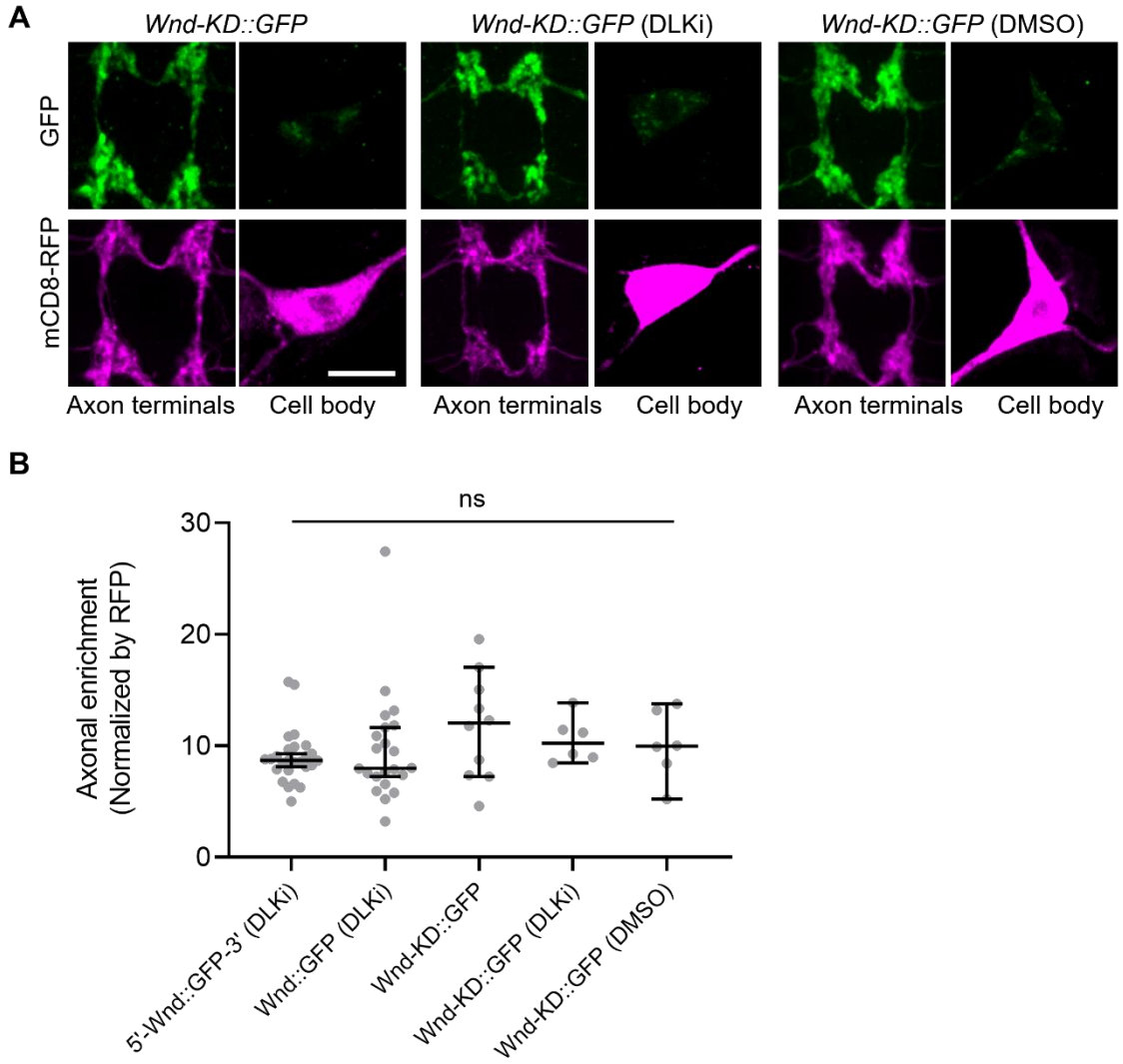

Figure 1- Supplement. The axon terminal enrichment of Wnd is independent of Wnd kinase activity.

(A) A Wnd kinase-dead (Wnd-KD::GFP, green) along with mCD8::RFP (magenta) were expressed in the larval C4da neurons in either regular food, food containing DMSO (vehicle control) or DLKi. The expression levels of transgenes were shown in C4da cell body and the axon terminals. Scale bar = 10 μm.

(B) The axonal enrichment index from Figure 1 and supplement 1 were expressed as median ± 95% CI. Genotypes and sample numbers were 5'-Wnd::GFP-3' (*w^{1118}; UAS-wnd-5'UTR-Wnd::GFP-wnd-3'UTR/+;ppk-GAL4, UAS-mCD8::RFP/+*) with DLKi (n = 26), Wnd::GFP (*w^{1118}; UAS-Wnd::GFP-SV40 3'UTR /+; ppk-GAL4, UAS-mCD8::RFP/+*) with DLKi (n = 22), Wnd-KD::GFP (*w^{1118}; UAS-Wnd-KD::GFP/+; ppk-GAL4, UAS-mCD8::RFP/+*) (n = 10), with DLKi (n = 6), with DMSO (n = 6); One-way ANOVA ($F(4,65) = 1.017$) followed by post hoc Tukey's multiple comparison test.

Figure 2

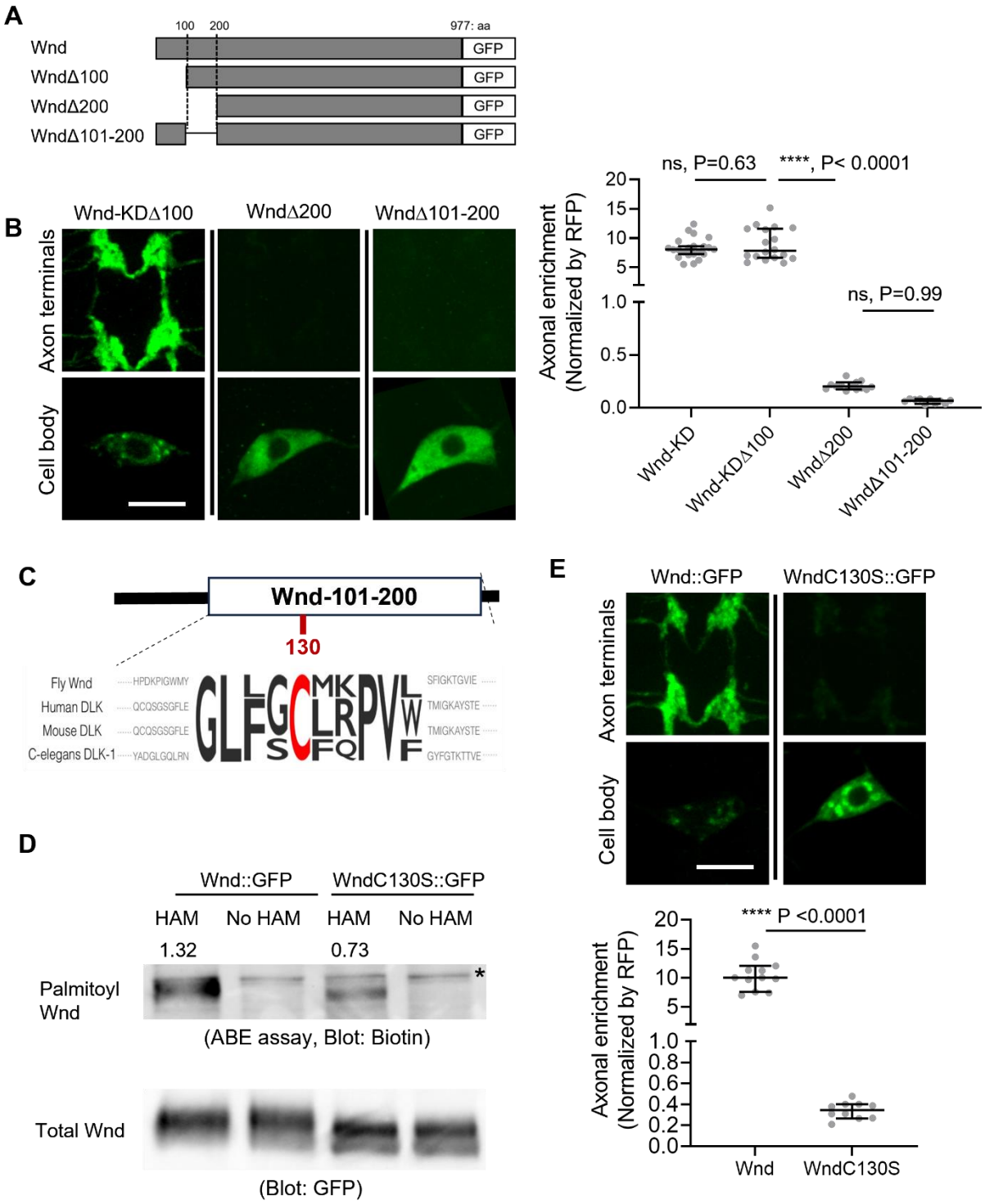
A
100
200
977: aa
Wnd
WndΔ100
WndΔ200
WndΔ101-200
GFP
B
Wnd-KDΔ100
WndΔ200
WndΔ101-200
Axon terminals
Cell body
ns, P=0.63
****, P< 0.0001
ns, P=0.99
Axonal enrichment
(Normalized by RFP)
Wnd-KD
Wnd-KDΔ100
WndΔ200
WndΔ101-200
C
Wnd-101-200
130
Fly Wnd
Human DLK
Mouse DLK
C-elegans DLK-1
D
Wnd::GFP
WndC130S::GFP
HAM
No HAM
1.32
0.73
Palmitoyl Wnd
(ABE assay, Blot: Biotin)
Total Wnd
(Blot: GFP)
E
Wnd::GFP
WndC130S::GFP
Axon terminals
Cell body
**** P <0.0001
Axonal enrichment
(Normalized by RFP)
Wnd
WndC130S

Figure 2. Wnd palmitoylation is essential for Wnd axonal localization.

(A) Schematic of Wnd deletion mutants. Deletion of the N-terminal 1-100aa of Wnd (WndΔ100), Deletion of the N-terminal 1-200 aa of Wnd (WndΔ200), and Deletion of the N-terminal 101-200 aa of Wnd (WndΔ101-200).

(B) The transgenes of serially deleted Wnd (green) along with mCD8::mRFP were expressed in the larval C4da neurons. Note that WndΔ100 was further mutated to remove kinase activity (Wnd-KDΔ100). The expression levels of Wnd::GFP proteins in C4da cell body and the axon terminals were shown (left). Scale bars = 10 μm. The axonal enrichment of each Wnd transgenes was measured using mCD8::RFP (not shown in figure) as a normalization control and expressed as median ± 95% CI. One-way ANOVA ($F_{(3,59)} = 103.8$) followed by post hoc Tukey's multiple comparison test. The p values from Tukey's test are indicated in the graph. Genotypes and sample numbers were Wnd-KD (*UAS-Wnd-KD::GFP/+;ppk-Gal4, UAS-mCD8::RFP/+*, n=22), Wnd-KDΔ*100* (*UAS-Wnd-KDΔ100::GFP/+;ppk-Gal4, UAS-mCD8::RFP/+*, n=18), WndΔ*200* (*UAS-WndΔ200::GFP/+;ppk-Gal4, UAS-mCD8::RFP/+*, n=13), and WndΔ*101-200* (*UAS-WndΔ101-200::GFP/+;ppk-Gal4, UAS-mCD8::RFP/+*, n=10).

(C) Wnd-C130 is an evolutionarily conserved palmitoylation site. The protein sequence alignment of DLK proteins from the indicated species is shown. The conserved Cysteine residue is shown in red.

(D) GFP-tagged Wnd proteins were expressed in S2 cells before pulled down by GFP nanobody beads. The Acyl Biotin Exchange assay was performed on the beads coupled Wnd proteins. Wnd-C130S::GFP is a palmitoylation defective version of Wnd. "No HAM" serves as a negative control since Biotin exchange does not occur in the absence of HAM. Biotin blot shows protein palmitoylation levels while total Wnd shows Wnd protein levels in the pulldown. The numbers indicate the total intensity of palmitoylation blot that were normalized by GFP blot from Wnd::GFP and Wnd-C130S::GFP.

(E) A wild-type Wnd::GFP transgene (Wnd::GFP) and a palmitoylation-defective Wnd transgene (Wnd-C130S::GFP) along with mCD8::RFP were expressed in the larval C4da neurons in the presence of DLKi. GFP immunostaining from Wnd::GFP proteins in C4da cell body and the axon terminals were shown (top). Scale bar = 10 μm. The axonal enrichment of the Wnd transgenes was measured using mCD8::RFP (not shown in figure) as a normalization control and expressed as median ± 95% CI (U=0, P<0.0001, two-tailed Mann-Whitney test). Genotypes and samples numbers were Wnd::GFP (*UAS-Wnd::GFP/+;ppk-Gal4, UAS-mCD8::RFP/+* , n = 12) and Wnd-C130S::GFP (*UAS-WndC130S::GFP/+;ppk-Gal4, UAS-mCD8::RFP/+* , n=10).

Figure 2 – supplement 1

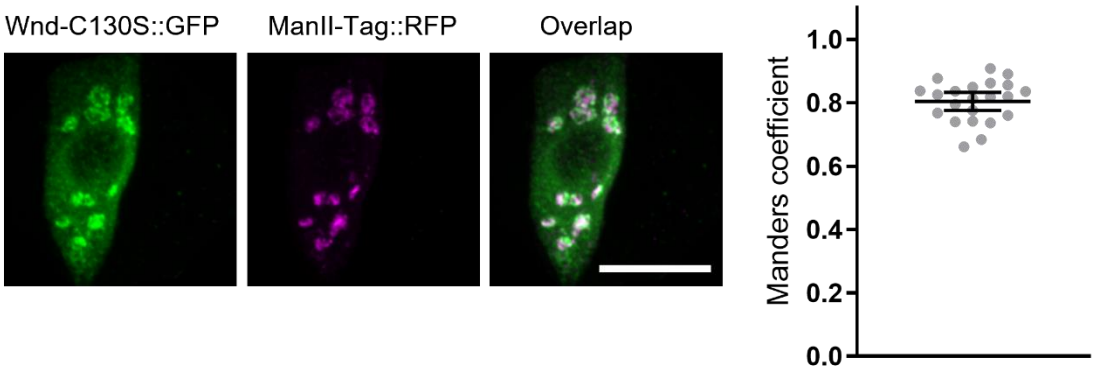

Figure 2 - Supplement 1. Wnd palmitoylation is not required for Wnd localization in somatic Golgi complex.

Wnd-C130S::GFP (green) along with a Golgi marker, ManII-Tag::RFP (magenta) were expressed in the larval C4da neurons. The expression patterns of the two transgenes in C4da cell bodies were shown (left). Scale bar = 10 μm. The Manders' overlap coefficient between Wnd transgenes and ManII-Tag::RFP was measured and expressed as median ± 95% CI (right). The Genotype and sample numbers were Wnd-C130S::GFP (*w^{1118}; UAS-Wnd-C130S-KD::GFP/+;ppk-GAL4/UAS-ManII-Tag-RFP*, n=22).

Figure 2 – supplement 2

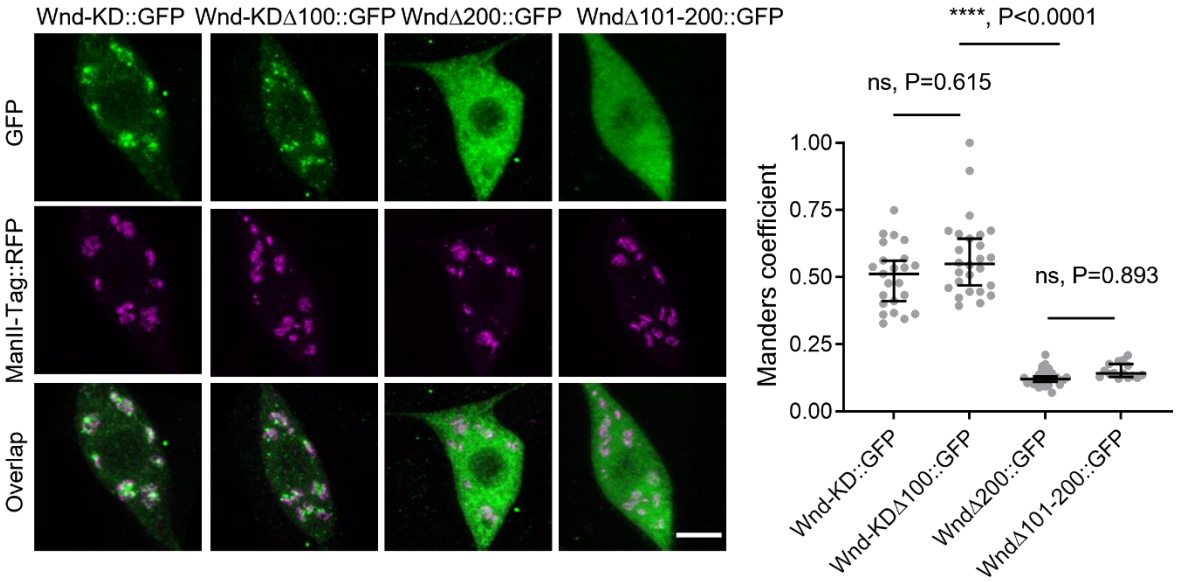

Figure 2 - Supplement 2. Somatic Golgi localization is necessary for Wnd localization in axon terminals.

Wnd transgenes (green) along with a Golgi marker, ManII-Tag::RFP (magenta) were expressed in the larval C4da neurons. The expression patterns of the two transgenes in C4da cell bodies were shown (left). Scale bar = 5 μm. The Manders' overlap coefficient between Wnd transgenes and ManII-Tag::RFP was measured and expressed as median ± 95% CI (right). Genotypes and sample numbers were Wnd-KD::GFP (*w^{1118}; UAS-Wnd-KD::GFP/+;ppk-GAL4/UAS-ManII-Tag-RFP*, n = 23), Wnd-KDΔ100::GFP (*w^{1118}; UAS-Wnd-Δ100-KD::GFP/+;ppk-GAL4/UAS-ManII-Tag-RFP*, n=26), Wnd-Δ200::GFP (*w^{1118};UAS-Wnd-Δ200::GFP/+;ppk-GAL4/UAS-ManII-Tag-RFP*, n=28) and Wnd-Δ101-200::GFP (*w^{1118};UAS-WndΔ101-200::GFP/+;ppk-GAL4/UAS-ManII-Tag-RFP*, n = 15). One-way ANOVA (F(3,88) = 129.8) followed by post hoc Tukey's multiple comparison test. The p values from Tukey's test are indicated in the graph.

Figure 2 – supplement 3

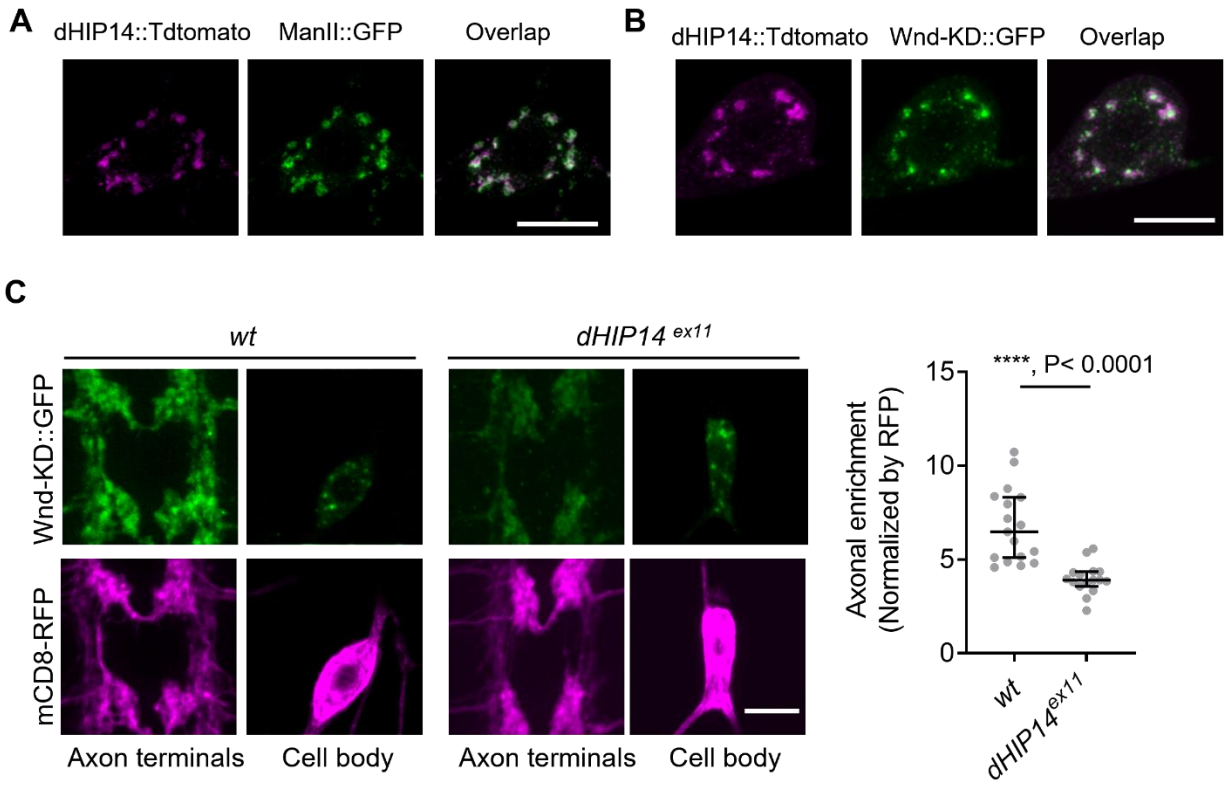

Figure 2 - Supplement 3. dHIP14 is required for Wnd localization in axon terminals.

(A) A Golgi marker, ManII::GFP (green) was expressed in the larval C4da neurons along with dHIP14::Tdtomato (magenta). The image was taken from a C4da cell body. Scale bar = 10 μm.
(B) Wnd-KD::GFP (green) was expressed in the larval C4da neurons along with dHIP14::Tdtomato (magenta). The image was taken from a C4da cell body. Scale bar = 10 μm.

(C) Wnd-KD::GFP (green) along with mCD8::RFP (magenta) were expressed in the larval C4da neurons from wild-type (*wt*) or homozygous *dHIP14* mutants (*dHIP14*^{ex11}). Scale bar = 10μm. The axonal enrichment of Wnd-KD::GFP was measured and expressed as a median ± 95% CI (Mann-Whitney U=13, P<0.0001, two-tailed Mann-Whitney test). Genotypes and sample numbers were *wt* (*UAS-Wnd-KD::GFP/ppk-Gal4, U-mCD8::RFP;+/+*, n=17) and *dHIP14*^{ex11}(*UAS-Wnd-KD::GFP/ppk-Gal4, U-mCD8::RFP;dHIP14*^{ex11}, n=16).

Figure 3

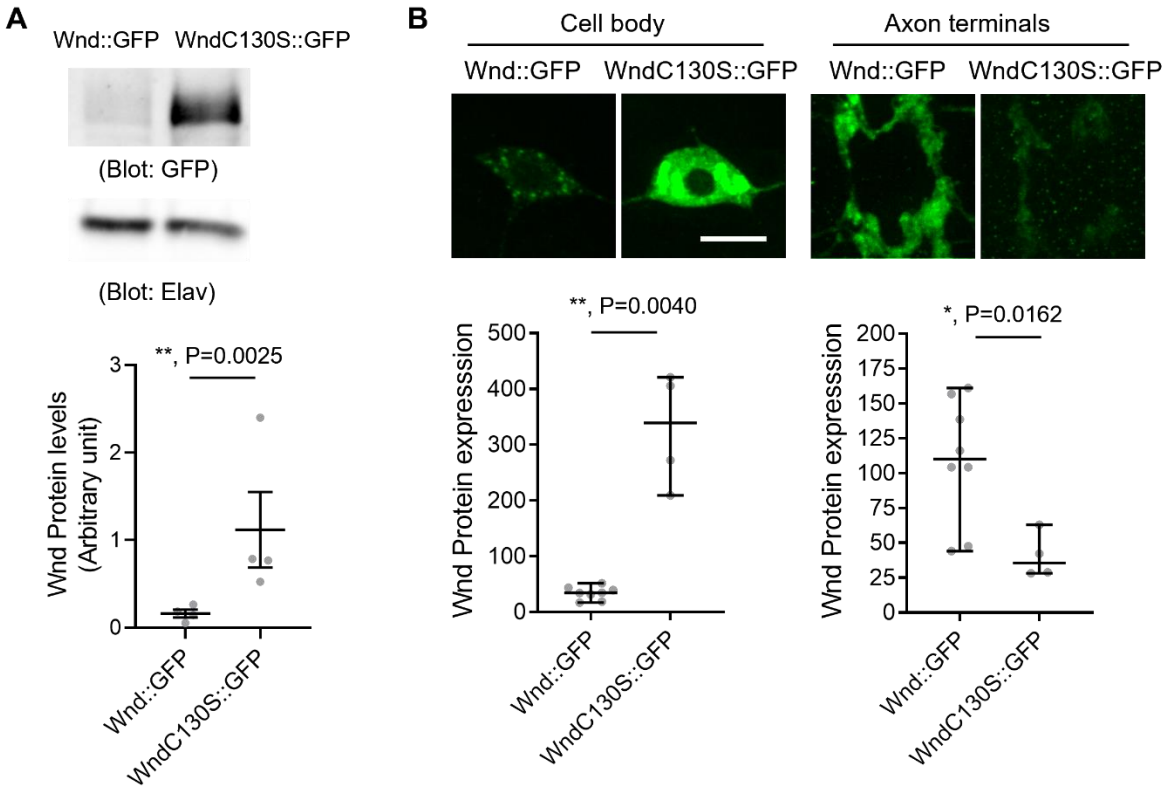

Figure 3. Increased protein expression levels of palmitoylation-defective Wnd.

(A) Wnd::GFP and Wnd-C130S::GFP were expressed in the larval nervous system using a pan-neuronal driver, *Elav*-GAL4 in the presence of DLKi. Larval brain lysates were subjected to Western blot analysis using a GFP antibody. Elav blot was used as a loading control. The GFP blots were normalized by Elav blots and expressed as mean ± SEM (n = 4, t = 9.409, df =3, p=0.0025, two-tailed ratio paired t-test). Genotypes were Wnd::GFP (*elav-Gal4/+; UAS-Wnd::GFP/+;*) and WndC130S::GFP (*elav-Gal4/+; UAS-WndC130S::GFP/+;*).

(B) Wnd transgenes (green) along with mCD8::RFP were expressed in the larval C4da neurons to directly compare the expression levels of Wnd::GFP and Wnd-C130S::GFP in C4da cell bodies and axon terminals. The larvae were treated with DLKi. Scale bar = 10 μm. The average fluorescent intensities from GFP staining of each larva sample (C4da cell bodies and axon terminals) were measured and expressed as median ± 95% CI (Axon terminal: Mann-Whitney U=2, P=0.0162, two-tailed Mann-Whitney test, Cell body: Mann-Whitney U=0, P<0.0001, two-tailed Mann-Whitney test). Genotypes and sample numbers were Wnd::GFP (*UAS-Wnd::GFP/+;ppk-Gal4, UAS-mCD8::RFP/+*, n = 8) and Wnd-C130S::GFP (*UAS-WndC130S::GFP/+;ppk-Gal4, UAS-mCD8::RFP/+*, n = 4).

Figure 4

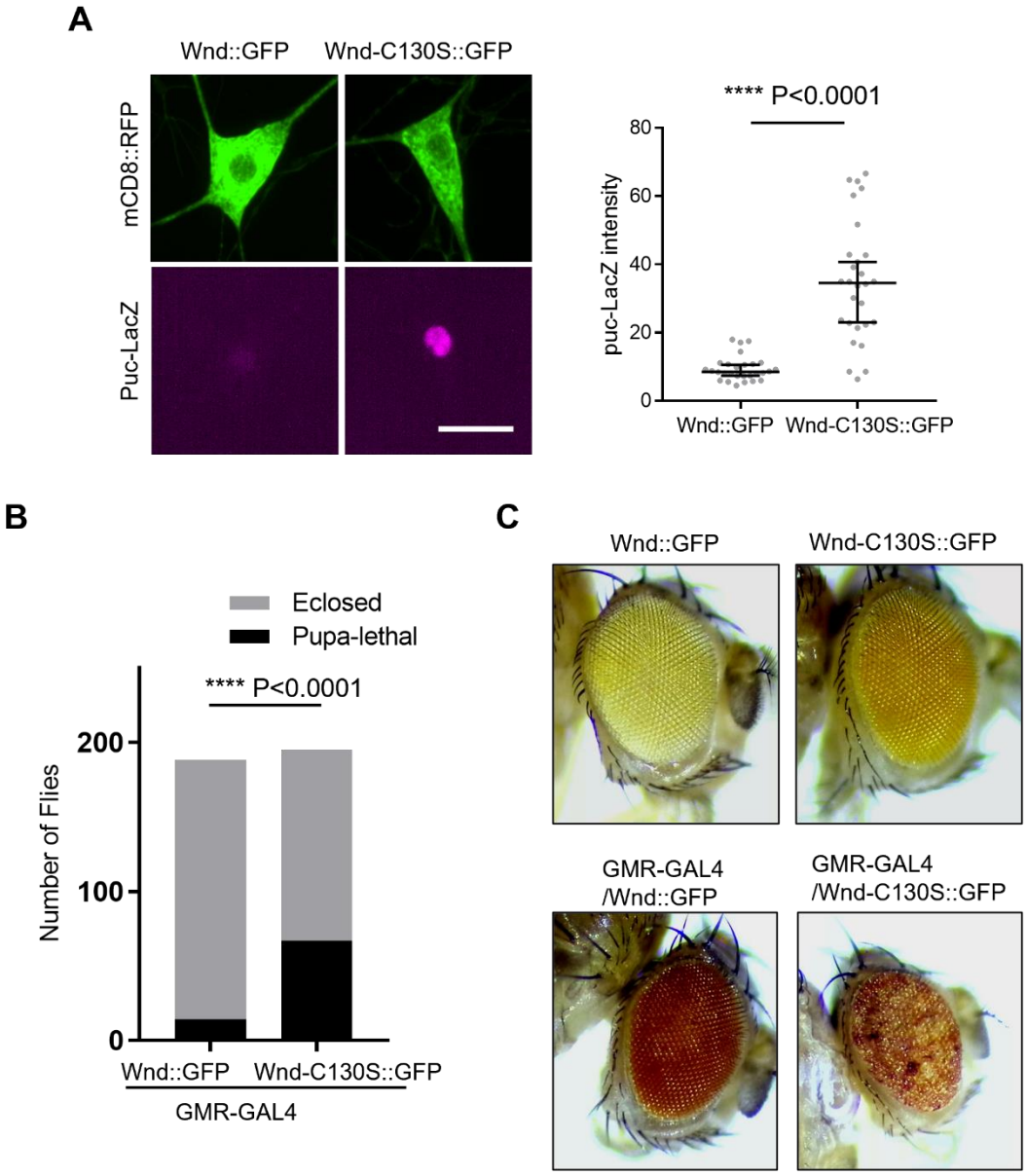

Figure 4. Palmitoylation-defective Wnd caused exacerbated stress responses.

(A) *puc*-LacZ were expressed along with *2XUAS-Wnd::GFP* and *2XUAS-Wnd-C130S::GFP* in the larval C4da neurons. The average fluorescent intensities from *puc*-LacZ staining of each larva sample in C4da cell body were measured and expressed as median ± 95% CI (Mann-Whitney U=56, P<0.0001, two-tailed Mann-Whitney test). Genotypes and sample numbers were 2XUAS-Wnd::GFP (*2XUAS-Wnd::GFP/ppk-Gal4,UAS-mCD8::RFP ;puc-LacZ/*+, n = 28) and 2XUAS-Wnd-C130S::GFP (*2XUAS-Wnd-C130S::GFP/ ppk-Gal4,UAS-mCD8::RFP ;puc-LacZ/*+, n = 28) Scale bar = 10 μm.

(B) *2XUAS-Wnd::GFP* and *2XUAS-Wnd-C130S::GFP* were expressed under an eye specific driver, *GMR-GAL4*. Adult fly lethality was scored and analyzed using the Chi-square (df =

41.57,1, z= 6.448, $p<0.0001$, two-sided contingency test). Genotypes and sample numbers were Wnd::GFP (*2XUAS-Wnd::GFP/GMR-Gal4*, n = 188), Wnd-C130S::GFP (*2XUAS-Wnd-C130S::GFP/GMR-Gal4*, n = 195).

(C) Representative images of fly eyes from Wnd::GFP (*2XUAS-Wnd::GFP/+*), Wnd-C130S::GFP (*2XUAS-Wnd-C130S::GFP/+*), Wnd::GFP under GMR-GAL4 (*2XUAS-Wnd::GFP/GMR-Gal4*), Wnd-C130S::GFP under GMR-GAL4 (*2XUAS-Wnd-C130S::GFP/GMR-Gal4*).

Figure 4 – supplement 1

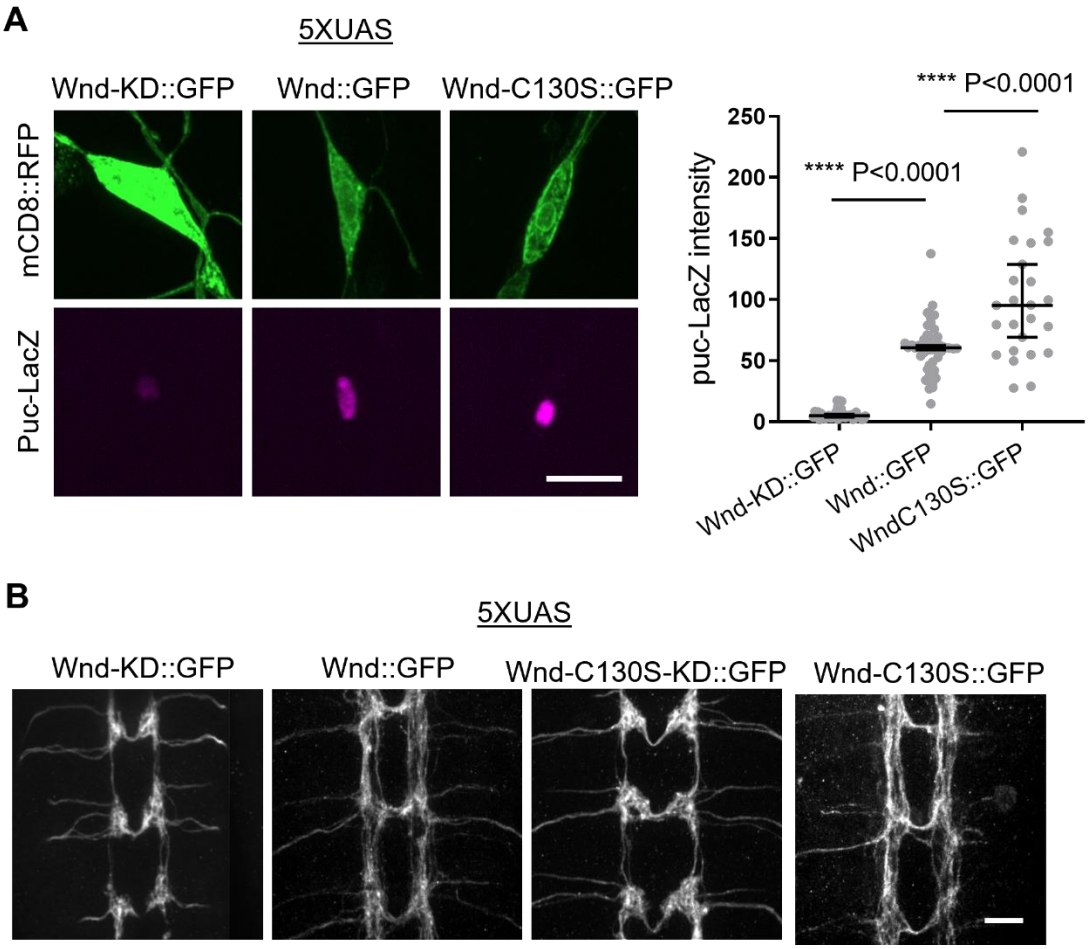

Figure 4 - Supplement 1. Wnd-C130S::GFP retains Wnd signaling capacity.

(A) *puc*-LacZ were expressed along with *5XUAS-Wnd-KD::GFP, 5XUAS-Wnd::GFP* and *5XUAS-Wnd-C130S::GFP* in the larval C4da neurons. The average fluorescent intensities from *puc*-LacZ staining of each larva sample in C4da cell body were measured and expressed as median ± 95% CI (One-way ANOVA, F (2, 114) = 108.3). Genotypes and sample numbers were 5XUAS-Wnd-KD::GFP (*;ppk-Gal4,UAS-mCD8::RFP/5XUAS-Wnd-KD::GFP;puc-LacZ/*+, n = 42), 5XUAS-Wnd::GFP (*;ppk-Gal4,UAS-mCD8::RFP/5XUAS-Wnd::GFP;puc-LacZ/*+, n = 49), and 5XUAS-Wnd-C130S::GFP (*;ppk-Gal4,UAS-mCD8::RFP/5XUAS-Wnd-C130S::GFP;puc-LacZ/*+, n = 26) Scale bar = 10 μm.

(B) Wnd transgenes along with mCD8::RFP were expressed in the larval C4da neurons using *ppk-GAL4*. The axon terminal morphology was visualized by mCD8::RFP. Wnd-KD::GFP (*UAS-Wnd-KD::GFP/+;ppk-Gal4, UAS-mCD8::RFP/*+), Wnd::GFP(*UAS-Wnd::GFP/+;ppk-Gal4, UAS-mCD8::RFP/*+), WndC130S::GFP (*UAS-WndC130S::GFP/+;ppk-Gal4, UAS-mCD8::RFP/*+) and WndC130S-KD::GFP (*UAS-WndC130S-KD::GFP/+;ppk-Gal4, UAS-mCD8::RFP/*+). Scale bar = 10 μm.

Figure 4 – supplement 2

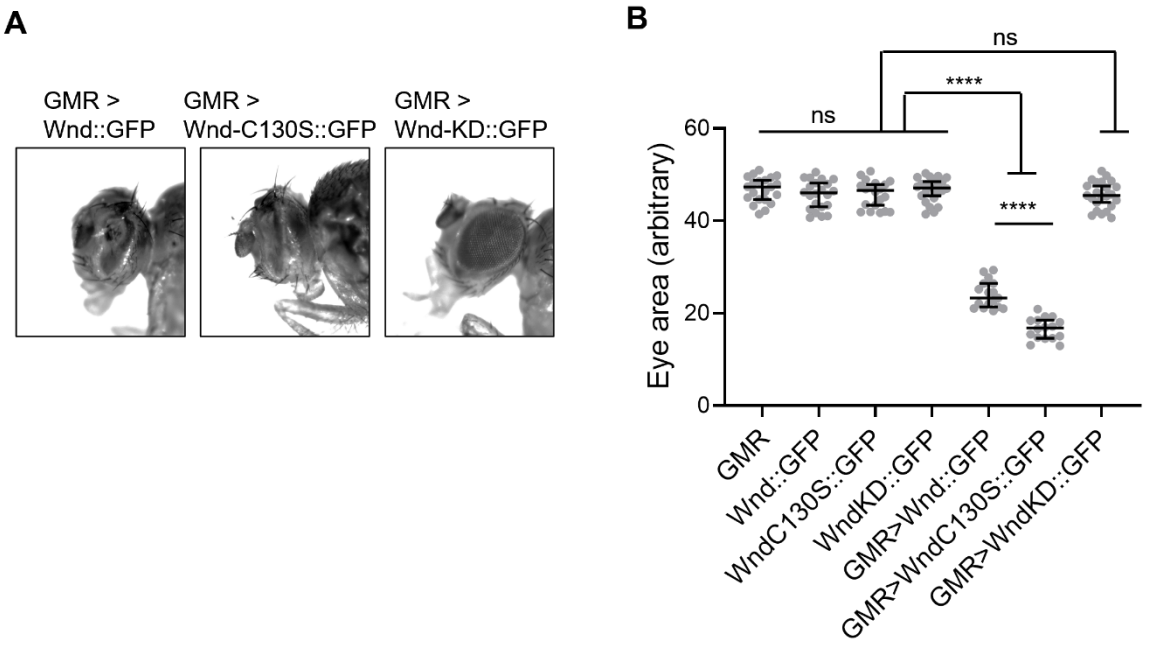

Figure 4 - Supplement 2. Wnd-C130S::GFP exhibits higher toxicity levels than Wnd::GFP.

(A) Representative images of fly eyes from Wnd::GFP under GMR-GAL4 (*GMR>Wnd::GFP*), Wnd-C130S::GFP under GMR-GAL4 (*GMR>Wnd-C130::GFP*), and Wnd-KD::GFP under GMR-GAL4 (*GMR>Wnd-KD::GFP*). Flies were reared at 18˚C.

(B) Eye area was quantified and expressed as median ± 95% CI. One-way ANOVA ($F(6, 136) = 362.0$) followed by post hoc Tukey's multiple comparison test (****, $P < 0.0001$). Genotypes and sample numbers were GMR (*GMR-GAL4/+*, n = 21), Wnd::GFP (*UAS-Wnd::GFP/+*, n = 22), Wnd-C130S::GFP (*UAS-Wnd-C130S::GFP/+*, n = 20), Wnd-KD::GFP (*UAS-Wnd-KD::GFP/+*, n = 24), GMR>Wnd::GFP (*GMR-GAL4/UAS-Wnd::GFP*, n = 17), GMR>Wnd-C130S::GFP (*GMR-GAL4/UAS-Wnd-C130S::GFP*, n = 16), and GMR>Wnd- KD::GFP (*GMR-GAL4/UAS-Wnd-KD::GFP*, n = 23). Note more severe eye phenotypes in GMR>Wnd-C130S::GFP as compared to GMR>Wnd::GFP.

Figure 5

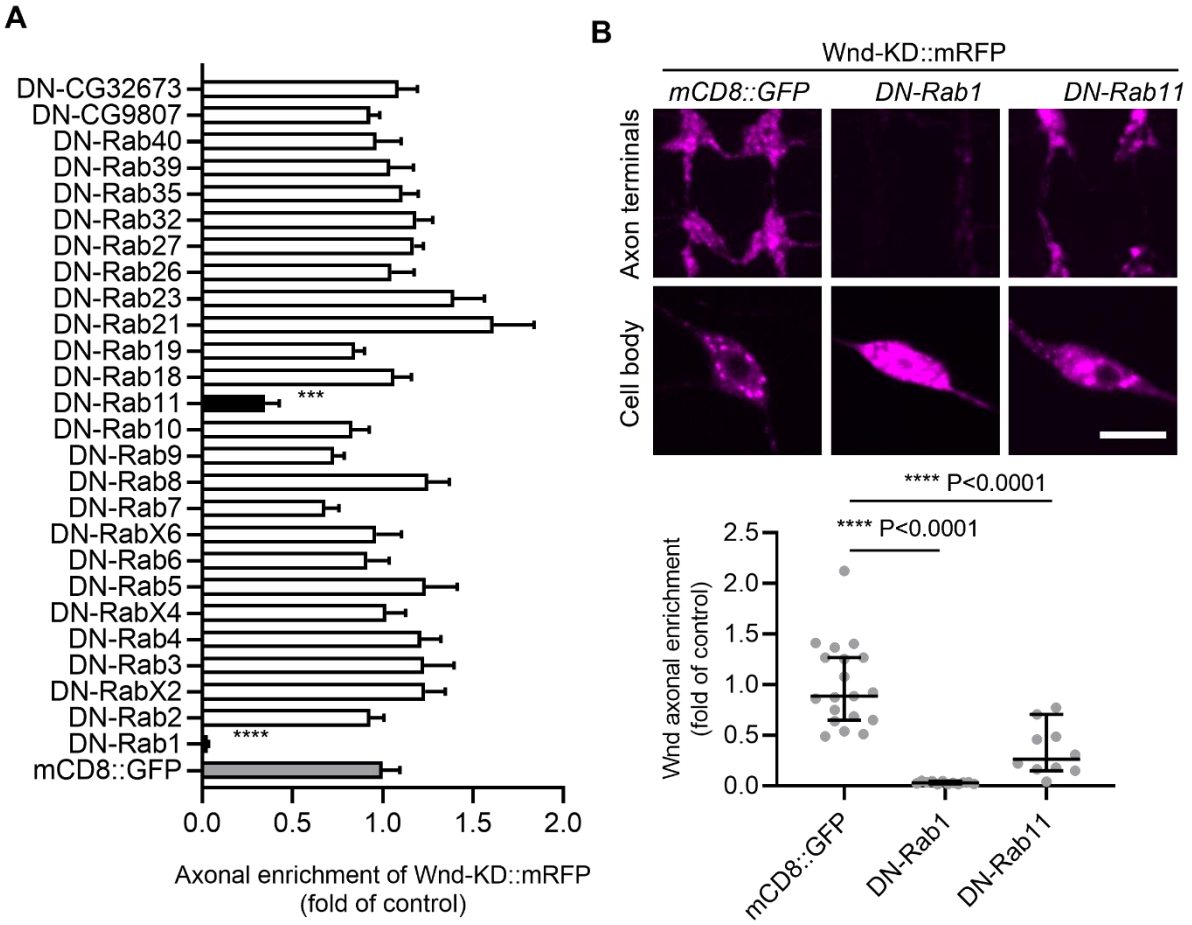

Figure 5. Screening of Dominant negative Rab proteins for Wnd axonal enrichment.

(A) YFP-tagged dominant negative-Rab (DN-Rab) transgenes along with Wnd-KD::mRFP were expressed in the larval C4da neurons. The axonal enrichment of Wnd-KD::mRFP was measured by Wnd-KD::mRFP expression levels from C4da cell bodies and axon terminals and expressed as mean ± sem of a fold change of control (mCD8::GFP) (n ≥10). One way ANOVA followed by post hoc Dunnett test ($F_{(27,284)} = 7.146$). A mCD8::GFP transgene was used as a transgene control (*UAS-Wnd-KD::mRFP/+;ppk-Gal4, UAS-mCD8::GFP*/+). Note that YFP::DN-Rab1 and YFP::DN-Rab11 reduced Wnd axonal enrichment by more than 50% compared to the control (gray bar).

(B) Representative images of Wnd-KD::mRFP expression in the axon terminals and cell bodies from the C4da neurons that express mCD8::GFP, DN-Rab1, and DN-Rab11 were shown. The Wnd axonal enrichment was expressed as median ± 95% CI (Mann-Whitney U=0, P < 0.0001 for DN-Rab1, U=13, P<0.0001 for DN-Rab11, two-tailed Mann-Whitney test). Genotypes and sample numbers were mCD8::GFP (*UAS-Wnd-KD::mRFP/+;ppk-Gal4, UAS-mCD8::GFP*/+, n= 19) DN-Rab1 (*UAS-Wnd-KD::mRFP/+;ppk-Gal4/ UAST-YFP.Rab1 S25N*, n=12) and DN-Rab11 (*UAS-Wnd-KD::mRFP/ UASp-YFP.Rab11 S25N; ppk-Gal4/+*, n=10) Scale bar = 10 μm.

Figure 6

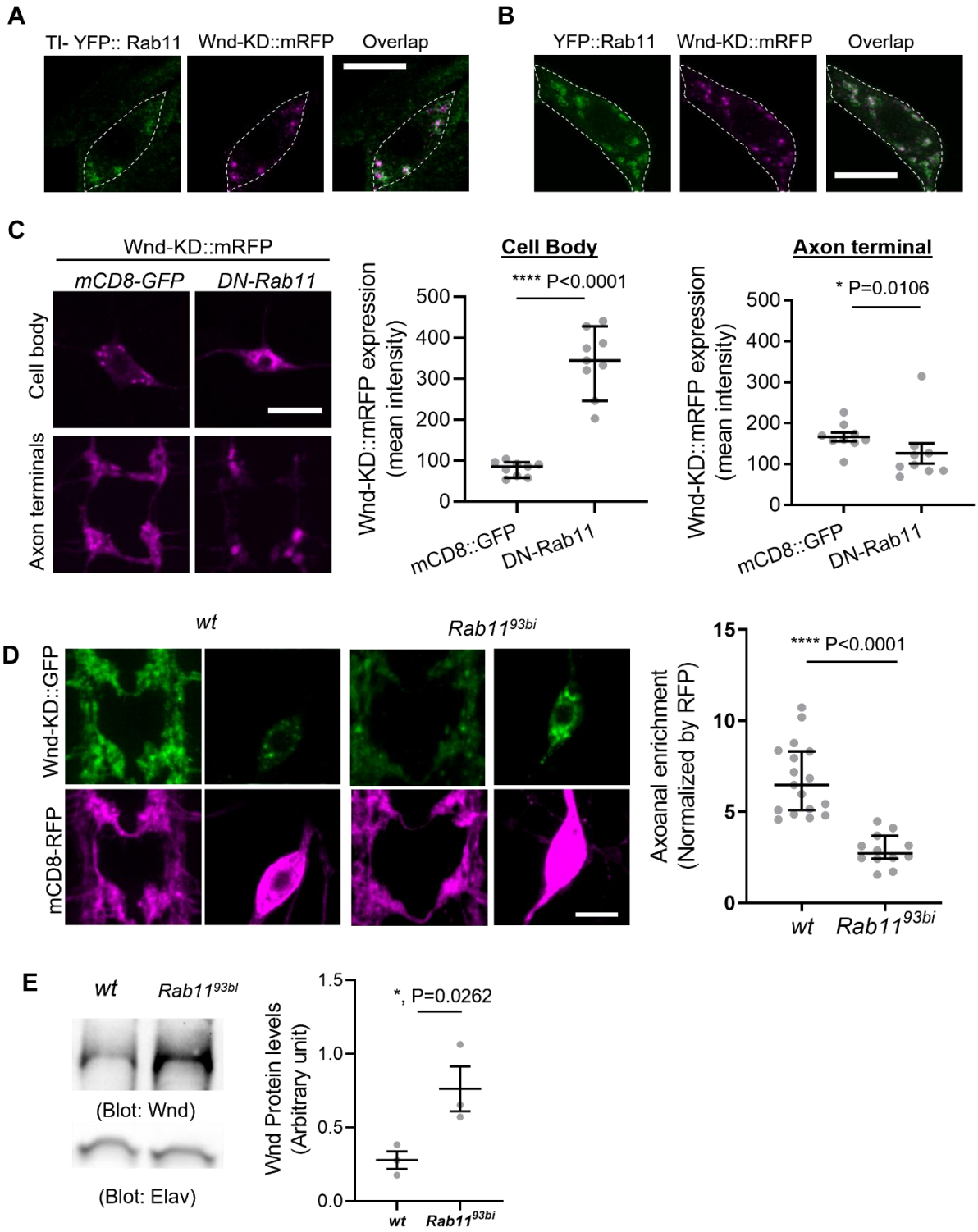
A
Tl- YFP:: Rab11
Wnd-KD::mRFP
Overlap
B
YFP::Rab11
Wnd-KD::mRFP
Overlap
C
Wnd-KD::mRFP
mCD8-GFP
DN-Rab11
Cell body
Axon terminals
Cell Body
**** P<0.0001
Wnd-KD::mRFP expression (mean intensity)
500
400
300
200
100
0
mCD8::GFP
DN-Rab11
Axon terminal
* P=0.0106
Wnd-KD::mRFP expression (mean intensity)
500
400
300
200
100
0
mCD8::GFP
DN-Rab11
D
wt
Rab11^93bi
Wnd-KD::GFP
mCD8-RFP
Axoanal enrichment (Normalized by RFP)
15
10
5
0
**** P<0.0001
wt
Rab11^93bi
E
wt
Rab11^93bl
(Blot: Wnd)
(Blot: Elav)
Wnd Protein levels (Arbitrary unit)
1.5
1.0
0.5
0.0
*, P=0.0262
wt
Rab11^93bi

Figure 6. Rab11 is necessary for Wnd localization in axon terminals and Wnd protein turnover.

(A) and (B). Wnd localizes at the Rab11-positive endosomes in C4da cell bodies.

Wnd-KD::mRFP was expressed in C4da neurons of *TI-YFP::Rab11* larvae (A). *TI-YFP::Rab11* is endogenously YFP-(Yellow fluorescent protein) tagged *Rab11* allele. Wnd-KD::mRFP was expressed in C4da neurons along with YFP::Rab11 (B). Wnd-KD::mRFP (magenta) and YFP::Rab11 (green) were visualized in C4da cell bodies using an RFP and GFP antibodies, respectively. Genotypes and sample numbers were *TI-YFP::Rab11* (*UAS-Wnd-KD::mRFP/+;TI{TI}Rab11[EYFP]/ppk-Gal4,* n=28) and *YFP::Rab11* (*UAS-Wnd-KD::mRFP/UAS-YFP::Rab11;ppk-Gal4/*+; , n=30). Scale bar = 10 μm.

(C) Wnd transgenes (magenta) along with mCD8::GFP or YFP::DN-Rab11 were expressed in the larval C4da neurons to directly compare the expression levels of Wnd-KD::mRFP in C4da cell bodies and axon terminals. Scale bar = 10 μm. The average fluorescent intensities from mRFP staining of each larva sample were measured and expressed as median ± 95% CI (Cell body: Mann-Whitney U=0, P <0.0001, two-tailed Mann-Whitney test; Axon terminal: Mann-Whitney U=12, P=0.0160, two-tailed Mann-Whitney test). Genotypes and sample numbers were *wt* (*UAS-Wnd-KD::mRFP/+;ppk-Gal4, UAS-mCD8::GFP/+,* n = 9) and *YFP::DN-Rab11* (*UAS-Wnd-KD::mRFP/UASp-YFP.Rab11.S25N ;ppk-Gal4, UAS-mCD8::RFP/*+, n = 9).

(D) Wnd-KD::GFP (green) along with mCD8::RFP (magenta) were expressed in the larval C4da neurons from wild-type (*wt*) or from homozygous *Rab11* mutants ($Rab11^{93bi}$). Images from C4da axon terminals and cell bodies were shown. Scale bar = 10 μm. The axonal enrichment of Wnd-KD::GFP was measured using mCD8::RFP as a normalization control and expressed as median ± 95% CI (Mann-Whitney U=0, P<0.0001, two-tailed Mann-Whitney test). Genotypes and sample numbers were *wt* (*UAS-Wnd-KD::GFP/ppk-Gal4, U-mCD8::RFP*, n=17) and $Rab11^{93bi}$ (*UAS-Wnd-KD::GFP/ppk-Gal4, U-mCD8::RFP;* $Rab11^{93bi}$, n=12).

(E) Western blot was performed on the larval brain lysates from wild-type (*wt,* w^{1118}) or homozygous $Rab11^{93bi}$ using Wnd antibody to measure total Wnd protein levels. Elav blot was used as a loading control. The Wnd blots were normalized by Elav blots and expressed as mean ± SEM (n = 3, t = 6.06, df =2, p=0.026, two-tailed ratio paired t-test).

Figure 6 – supplement 1

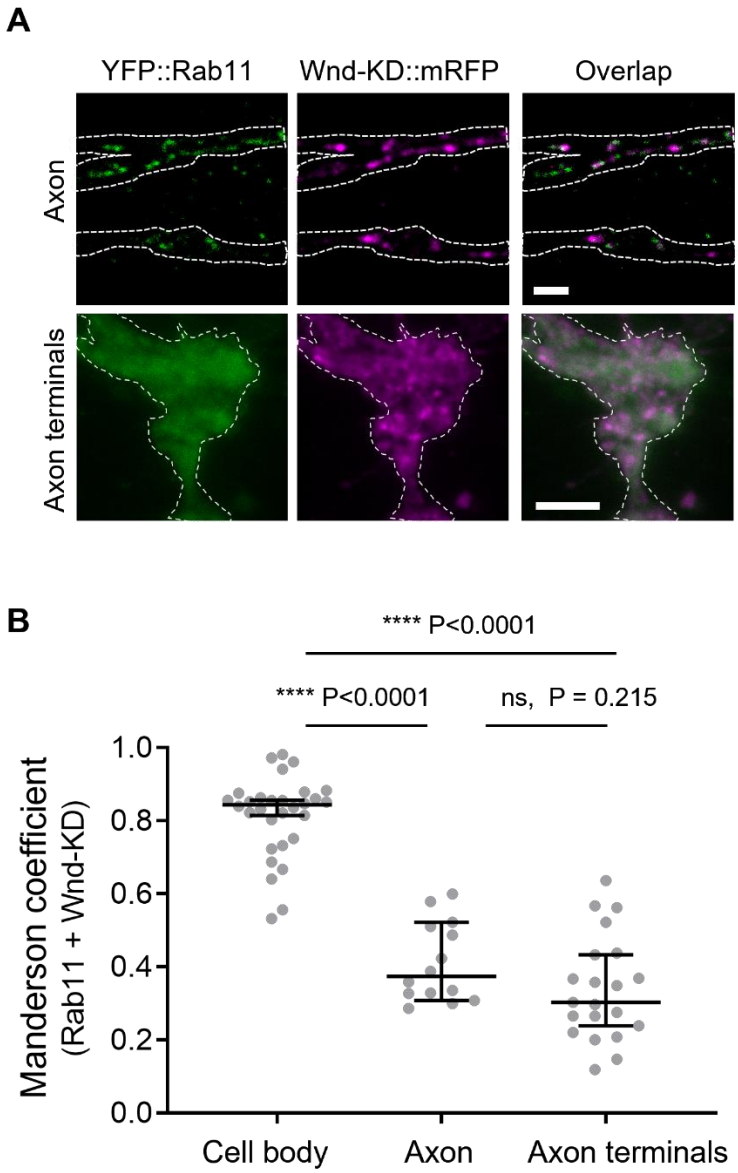

Figure 6 - Supplement 1. Wnd does not localize in the Rab11-positive endosomes in axons and axon terminals.

(A) Wnd-KD::mRFP and YFP::Rab11 were expressed in the larval C4da neurons using *ppk-GAL4*. Wnd-KD::mRFP (magenta) and YFP::Rab11 (green) were visualized in the segmental nerve/axons (top) and in C4da axon terminals (bottom) using RFP and GFP antibodies, respectively. Scale bar = 10 μm.

(B) The Manders' overlap coefficient between Wnd-KD::mRFP and YFP::Rab11 was measured in cell bodies, axons (segmental nerve), and axon terminals. They are expressed as median ± 95% CI. One-way ANOVA ($F(2, 62) = 109.8$) followed by post hoc Tukey's multiple comparison test. Sample numbers were; Cell body n=30, axons n = 14, neuropils n=21.

Figure 6 – supplement 2

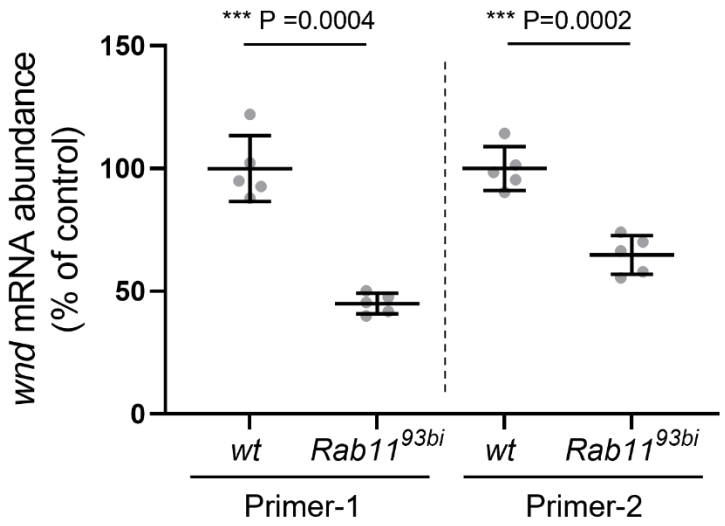

Figure 6 - Supplement 2. *Rab11* mutations did not increase *wnd* mRNA abundance.

Total RNAs extracted from the wondering third instar larval brains from a wild-type (*wt*) control (w^{1118}) and $Rab11^{93bi}$ were subjected to RT-qPCR to measure *wnd* mRNA abundance. The *wnd* mRNA levels were normalized by *GAPDH1* mRNA levels via the 2ΔΔCT method. Two independent wnd primer sets were used (Primer-1 and Primer-2). The data were expressed as mean ± SEM of five technical replicates. Welch's t-test (Primer-1: t=8.778, df=4.772, Primer-2: t=6.576, df=7.875).

Figure 7

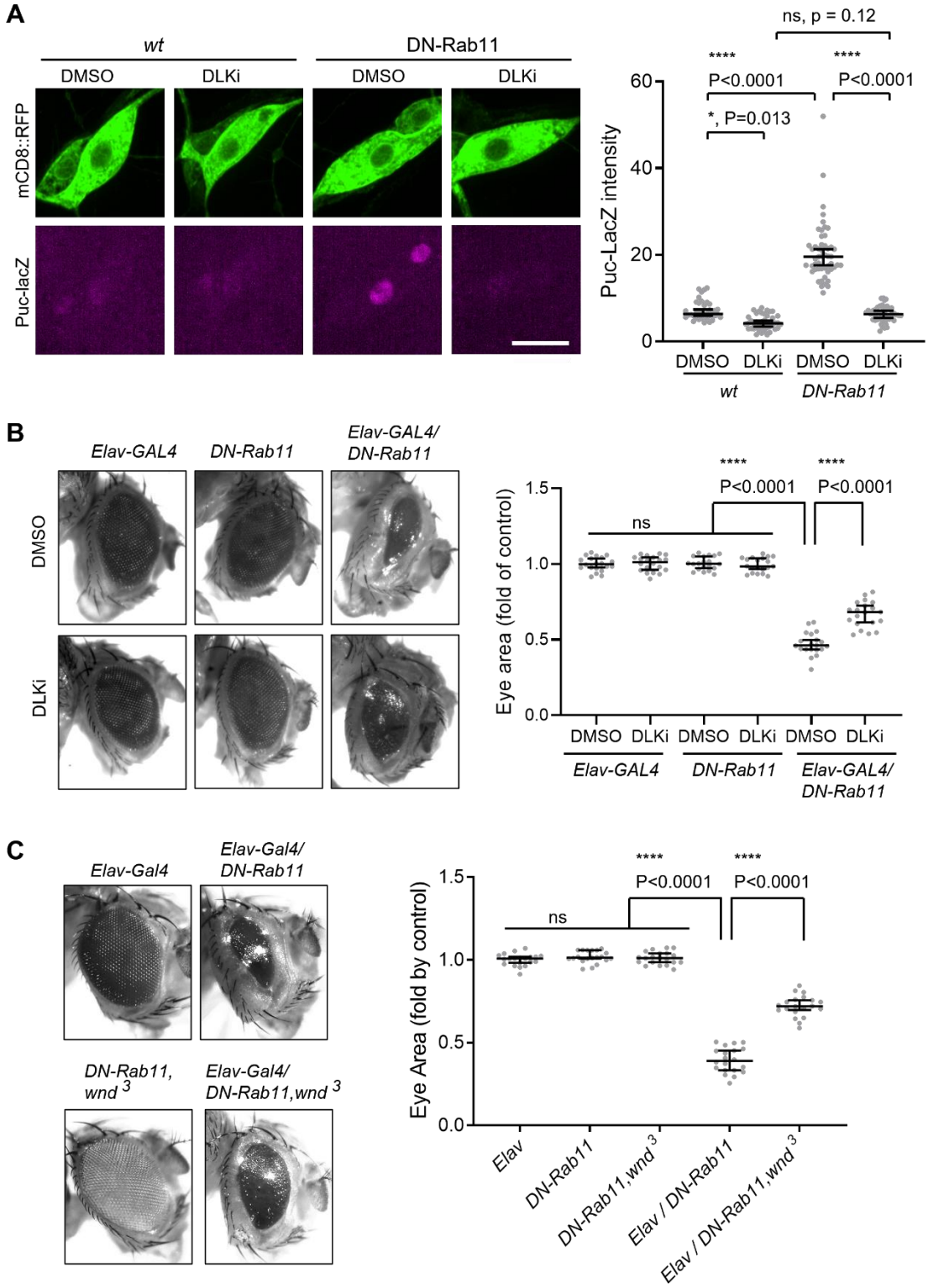
A
wt
DN-Rab11
DMSO
DLKi
DMSO
DLKi
mCD8::RFP
Puc-lacZ
ns, p = 0.12
****
****
P<0.0001
P<0.0001
*, P=0.013
Puc-LacZ intensity
60
40
20
0
DMSO
DLKi
DMSO
DLKi
wt
DN-Rab11
B
Elav-GAL4
DN-Rab11
Elav-GAL4/
DN-Rab11
DMSO
DLKi
****
****
P<0.0001
P<0.0001
ns
Eye area (fold of control)
1.5
1.0
0.5
0.0
DMSO
DLKi
DMSO
DLKi
DMSO
DLKi
Elav-GAL4
DN-Rab11
Elav-GAL4/
DN-Rab11
C
Elav-Gal4
Elav-Gal4/
DN-Rab11
DN-Rab11,
wnd 3
Elav-Gal4/
DN-Rab11,wnd 3
****
****
P<0.0001
P<0.0001
ns
Eye Area (fold by control)
1.5
1.0
0.5
0.0
Elav
DN-Rab11
DN-Rab11,wnd 3
Elav / DN-Rab11
Elav / DN-Rab11,wnd 3

Figure 7. Wnd mediates stress signaling induced by Rab11 loss-of-function.

(A) *puc*-LacZ were expressed along with YFP::DN-Rab11 and mCD8::GFP in the larval C4da neurons in the presence of DMSO (vehicle) or DLK inhibitor (DLKi). The average fluorescent intensities from LacZ staining of each larva sample in C4da cell bodies were measured and quantified as median ± 95% CI. One-way ANOVA (F (3,171) = 11.48) followed by post hoc Tukey's multiple comparison test (****, P < 0.0001). Genotypes and sample numbers were *wt (; ppk-Gal4, UAS-mCD8::RFP/+;puc-LacZ/*+, in DMSO, n = 36, in DLKi n=42) and DN-Rab11 (*; ppk-Gal4, UAS-mCD8::RFP/+;puc-LacZ/UASp-YFP.Rab11.S25N*, in DMSO, n = 51, in DLKi, n=46) Scale bar = 10 µm.

(B) Representative images of fly eyes from *Elav-GAL4* only, *DN-Rab11* only, and *DN-Rab11* expression under a pan-neuronal driver, *Elav-GAL4 (Elav-GAL4/DN-Rab11)*. Flies were reared in the presence of DMSO and DLKi (down). Eye area was quantified and expressed as median ± 95% CI. One-way ANOVA (F (5,114) = 290.3) followed by post hoc Tukey's multiple comparison test (****, P < 0.0001). Genotypes and sample numbers were Elav-Gal4 (*Elav-GAL4/*+, n = 20), DN-Rab11 (*;;UASp-YFP.Rab11.S25N/*+, n = 20), Elav-Gal4/DN-Rab11 (*ElavGal4/+;;UASp-YFP.Rab11.S25N /*+, n = 20).

(C) Representative images of fly eyes from *Elav-GAL4* only, *DN-Rab11* only in heterozygous *wnd* mutant (*DN-Rab11, wnd*^{3}), DN-Rab11 expression under a pan-neuronal driver, *Elav-GAL4* (*Elav-GAL4/DN-Rab11*), and DN-Rab11 expression under a pan-neuronal driver in heterozygous *wnd* mutant (*Elav-GAL4/DN-Rab11, wnd*^{3}). Eye area was quantified and expressed as median ± 95% CI. One-way ANOVA (F (4,95) = 530.4) followed by post hoc Tukey's multiple comparison test.

Figure 8

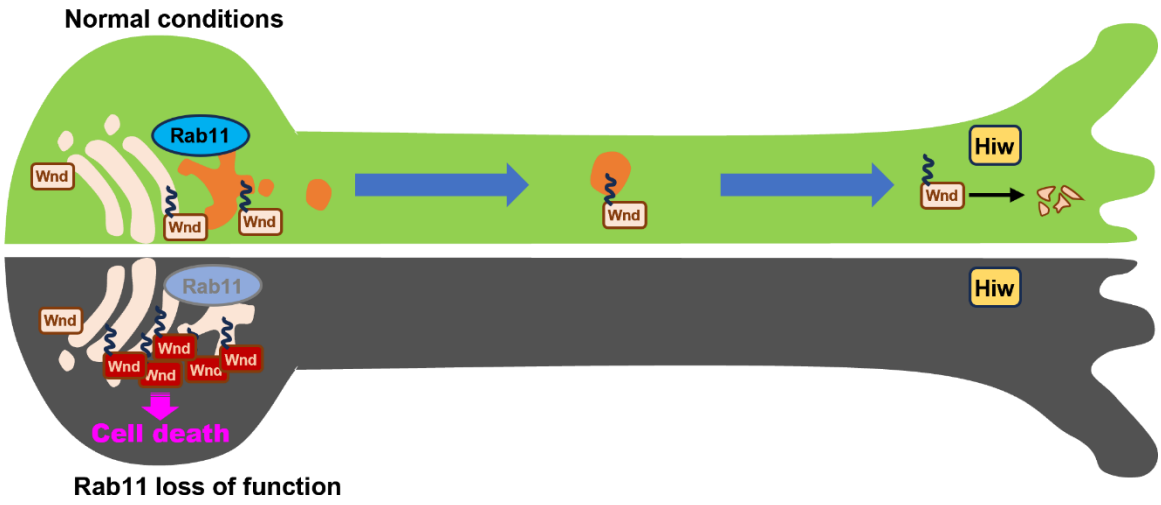

Figure 8. Rab11 suppresses neuronal stress signaling by localizing Dual leucine zipper kinase to axon terminals for protein turnover.

Under normal conditions, the newly synthesized Wnd proteins are recruited to the Golgi apparatus in neuronal cell body. Wnd is palmitoylated at somatic Golgi apparatus, which enables it to be sorted into the Recycling Endosomes via Rab11. Wnd is actively transported out of neuronal cell bodies towards axon terminals where Hiw-mediated degradation of Wnd occurs. When Rab11 function is lost, Wnd proteins cannot be transported towards axon terminals. This prevents Wnd protein turnover resulting in higher Wnd protein expression, which in turn triggers cell death pathway.

Table 1

REAGENT or RESOURCE	SOURCE	RRID
UAST-YFP.Rab1.S25N	Zhang et al., 2007	BDSC_9757
UAST-YFP.Rab2.S20N	Zhang et al., 2007	BDSC_23640
UASp-YFP.RabX2.S21N	Zhang et al., 2007	BDSC_9843
UASp-YFP.Rab3.T35N	Zhang et al., 2007	BDSC_9766
UASp-YFP.Rab4.S22N	Zhang et al., 2007	BDSC_9769
UAST-YFP.RabX4.T40N	Zhang et al., 2007	BDSC_9849
UASp-YFP.Rab5.S43N	Zhang et al., 2007	BDSC_9771
UAST-YFP.Rab6.T26N	Zhang et al., 2007	BDSC_23249
UAST-YFP.RabX6.S22N	Zhang et al., 2007	BDSC_9856
UASp-YFP.Rab7.T22N	Zhang et al., 2007	BDSC_9778
UASp-YFP.Rab8.T22N	Zhang et al., 2007	BDSC_9780
UASp-YFP.Rab9.S26N	Zhang et al., 2007	BDSC_23642
UASp-YFP.Rab10.T23N	Zhang et al., 2007	BDSC_9786
UASp-YFP.Rab11.S25N	Zhang et al., 2007	BDSC_9792
UAST-YFP.Rab18.S19N	Zhang et al., 2007	BDSC_23238
UAST-YFP.Rab19.T35N	Zhang et al., 2007	BDSC_9799
UAST-YFP.Rab21.T27N	Zhang et al., 2007	BDSC_23241
UASp-YFP.Rab23.S51N	Zhang et al., 2007	BDSC_9804
UAST-YFP.Rab26.T204N	Zhang et al., 2007	BDSC_9807
UASp-YFP.Rab27.T25N	Zhang et al., 2007	BDSC_23267
UASp-YFP.Rab32.T33N	Zhang et al., 2007	BDSC_23281
UAST-YFP.Rab35.S22N	Zhang et al., 2007	BDSC_9819
UAST-YFP.Rab39.S23N	Zhang et al., 2007	BDSC_23247
UAST-YFP.Rab40.H25N	Zhang et al., 2007	BDSC_9829
UAST-YFP.CG9807.T21N	Zhang et al., 2007	BDSC_23257
UAST-YFP.CG9807.T21N	Zhang et al., 2007	BDSC_23258
UAST-YFP.CG32673.T21N	Zhang et al., 2007	BDSC_23254
UASp-YFP.Rab11	Zhang et al., 2007	BDSC_50782
TI{TI}Rab11[EYFP]	Dunst et al., 2015	BDSC_62549
Rab11[93Bi]	Giansanti et al., 2007	BDSC_4158